Mineralogical and elemental geochemical characteristics of Taodonggou Group in Taibei Sag , Turpan-Hami Basin: Implication for Source sink system and evolution history of lake basin

Huan Miao[1,2*], Jianying Guo[3*], Yanbin Wang[4], Zhenxue Jiang[1,2], Chengju Zhang [1,2], Chuanming Li[1,5]

(1. State Key Laboratory of oil and gas resources and exploration, Beijing 102249, China;

2. Institute of unconventional oil and gas science and technology, China University of Petroleum (Beijing), Beijing 102249, China;

3. CNPC Key Laboratory of Natural Gas Accumulation and Development,Langfang 065007,China;

4 School of Geosciences and Surveying Engineering,China University of Mining and Technology(Beijing),Beijing 100083,China;

5. College of Geosciences, China University of Petroleum (Beijing), Beijing 102249, China;)

Corresponding author: Huan Miao1627765379@qq.com; Jianying Guo gjy_17711224@petrochina.com.cn

Abstract: The Middle Permian is an important basin-forming period in the Turpan-Hami Basin. Based on mineral characteristics and elemental geochemistry of the Taodonggou Group mudstone we analyze the parent rock type, source area location, sedimentary environment and source area tectonic background for this mudstone. On this basis we are able to reconstruct the source-sink system and lake basin evolution of the Taodonggou Group. We find the following: (1) Taodonggou Group mudstone minerals are mainly clay and quartz, and can be classified into four petrographic types according to mineral fraction. (2) The Taodonggou Group mudstone was deposited in a warm, humid and hot paleoclimate, with strong weathering. The parent rocks of the Taodonggou Group mudstone are two types of felsic volcanic rocks and andesites, with weak sedimentary sorting and recycling and with well-preserved source information. (3) The Taodonggou Group mudstone were deposited in dyoxic freshwater-brackish water in intermediate-depth or deep lakes with stable inputs of terrigenous debris but at slower deposition rates. Deposition of the middle of Taodonggou Group was influenced by hydrothermal activity; the tectonic setting of the Taodonggou Group source area was a continental island arc and an oceanic island arc. (4) The evolution of the Middle Permian Lake basin in the Turpan-Hami Basin can be divided into three stages: In the early part of the deposition of Taodonggou Group the depocenter was in the Bogda area. At this time the area that became Mt Bogda was not exposed and a succession of high-quality type-III source rocks was widely deposited in the basin. In the middle of the deposition of the Taodonggou Group the depocenter gradually migrated to the Taibei Sag. At this time the Mt Bogda area underwent uplift, and, together with hydrothermal activity, a succession of type-II source rocks was widely deposited in the basin. In the late part of the Taodonggou Group, uplift of the Mt Bogda area ceased and the depocenter transferred entirely to the Taibei Sag.

Keyword: Turpan-Hami Basin;Taodonggou Group;Mineralogy;Element Geochemistry;Sedimentary Environment;Source sink system

1 Introduction

The provenance analysis is a method to determine the provenance location, provenance type and transportation path of sediments, which is of great significance for restoring the sedimentary tectonic evolution process of the basin (McLennan et al., 1983; Kröner et al., 1985). There are many methods for provenance analysis, such as heavy and light mineral analysis, zircon U-Pb dating, isotope, petrology and element geochemistry (Rollinson, 1993; Roser and Korsch, 1988; Gehrels et al., 2008). Compared with traditional clastic rocks, mudstone belongs to a class of fine-grained sediments, and heavy mineral analysis and other means are difficult to apply. Therefore, element geochemical methods can be used to realize provenance analysis (Li et al., 2020). Element geochemical analysis is used to determine the lithology of source rock, the weathering degree and tectonic setting of sedimentary source area by analyzing the characteristics of major, trace element and rare earth element of mudstone in the sedimentary area (Li et al., 2020; Floyd and Leveridge, 1987; Basu et al, 2016). Previous studies have found that provenance not only affects the salinity change of lake water, but also affects the input of nutrients and terrestrial organic matter, thus affecting the quality of mudstone(Li et al., 2020; Deditius, 2015; Essefi, 2021). The tectonic activities in the provenance area not only affect the change of sedimentary center, but also affect the change of provenance area (Miao et al., 2022; Pinto et al., 2010). Therefore, it is of great significance to analyze the provenance and tectonic background of mudstone for reconstructing the sedimentary tectonic evolution history of the basin.

Turpan-Hami Basin, Junggar Basin and Bogda area all belong to the southern part of the ancient Asian ocean in the Paleozoic era (Korobkin and Buslov, 2011; Jiang et al., 2015). During the Early Carboniferous to Early Permian, they began momentous to separate due to the continuous expansion of the Bogda Rift and began to enter the basin-forming period in the Middle Permian (Miao et al., 2004; Novikov, 2013; Jiang et al., 2015; Wang et al., 2019; Zhang et al., 2019). The Middle Permian is a momentous stage in the tectonic evolution of the Turpan-Hami basin. During this period, the expansion of the Bogda Rift stopped. With the gradual withdrawal of seawater from Xinjiang, the sedimentary environment of Turpan-Hami basin gradually shifted to continental facies, and the sedimentary center gradually shifted from Bogda area to Taibei Sag (Miao et al., 2004; Shi et al., 2020; Li et al., 2022).Taodonggou Group mudstone are widely deposited in Turpan-Hami Basin. Previous studies have confirmed that Taodonggou Group mudstone is a very good - excellent source rock with huge hydrocarbon generation potential (Song et al., 2018; Miao et al., 2021; Miao et al., 2022; Miao et al., 2022; Miao et al., 2022).

The sedimentary environment of mud shale is closely related to its hydrocarbon generation potential (Wu et al., 2021; Li et al.,2022; Zhang et al., 2019; Zhao et al., 2021;Miao et al., 2004). Although previous scholars believed that the Taodonggou Group mudstone was deposited in a warm and humid paleoclimate, a high salinity water body, and a dyoxic environment by analyzing outcrop samples and biomarkers, these understandings are relatively simple (Miao et al., 2004; Song et al., 2018; Miao et al., 2021). In Turpan-Hami Basin, it is difficult to meet the requirements of the transfer of the Middle Permian sedimentary environment from marine to continental facies, and the transfer of the sedimentary center from the Bogda area

62   to Taibei Sag is a complicated process. Therefore, when reconstructing the sedimentary environment of Middle Permian

63   mudstone, its provenance information and tectonic setting should be considered.

64   Therefore, based on the mineralogical and elemental geochemical characteristics of 16 mudstone samples collected from

65   well YT1, this study analyzed the paleoclimate, paleosedimentary environment, provenance and tectonic setting of source

66   area of Taodonggou Group mudstone during the sedimentary period. The location of the source area of the Taodonggou Group

67   is determined, and the source-sink system of the Taodonggou Group mudstone and the evolution history of the Turpan-Hami

68   Basin are reconstructed.

69 **2 Geological setting**

70   Turpan-Hami Basin, located in the eastern part of Xinjiang Uygur Autonomous Region, is one of the three major

71   petroliferous basins in Xinjiang. It is 660 km long from east to west and 0~130 km wide from north to south, with a total

72   covered area of 5.35×10^4 km². The Turpan-Hami Basin has undergone four stages: extensional rift basin development stage,

73   compressional foreland basin development stage, extensional faulted basin development stage, and compressional regenerated

74   foreland basin development stage, and finally formed the current pattern of Mesozoic Cenozoic superimposed composite

75   inland basin (Zhu et al., 2009; Jiang et al., 2015; Wartes et al., 2002; Greene et al., 2005). According to the tectonic evolution

76   characteristics of the Turpan-Hami Basin, the Turpan-Hami Basin can be divided into three primary tectonic units from east

77   to west: Hami Depression, Liaodun Uplift and Turpan Depression (Miao et al.,2021; Fig. 1a).

78   Taibei sag, the secondary sag of Turpan depression in Turpan-Hami basin, is the largest sedimentary unit in Turpan-Hami

79   basin (Fig. 1b). The Taibei sag is a Paleozoic-Cenozoic inherited subsidence area (Li et al., 2021), which is a key area for oil

80   and gas exploration in the Turpan-Hami Basin due to its high thermal evolution degree of hydrocarbon source rocks, good

81   reservoir physical properties, good cap sealing, and rich oil and gas resources. which is the focus of oil and gas exploration

82   in the Turpan-Hami Basin. (Wu et al., 2021; Li et al., 2021). Taodonggou Group is the general name of Daheyan Formation

83   and Taerlang Formation. Due to the stratigraphic boundary between the Taerlang Formation and Daheyan Formation is not

84   obvious, it is collectively called the Taodonggou Group. The Middle Permian Taodonggou Group are mainly located in the

85   western part of the study area. At present, only YT1 and L30 wells are drilled (YT1 well is drilled through, L30 well is not

86   drilled through). The burial depth of the stratum is 4000~6500 m, and the thickness of mudstone is 50~200 m (Miao et al.,

87   2022).
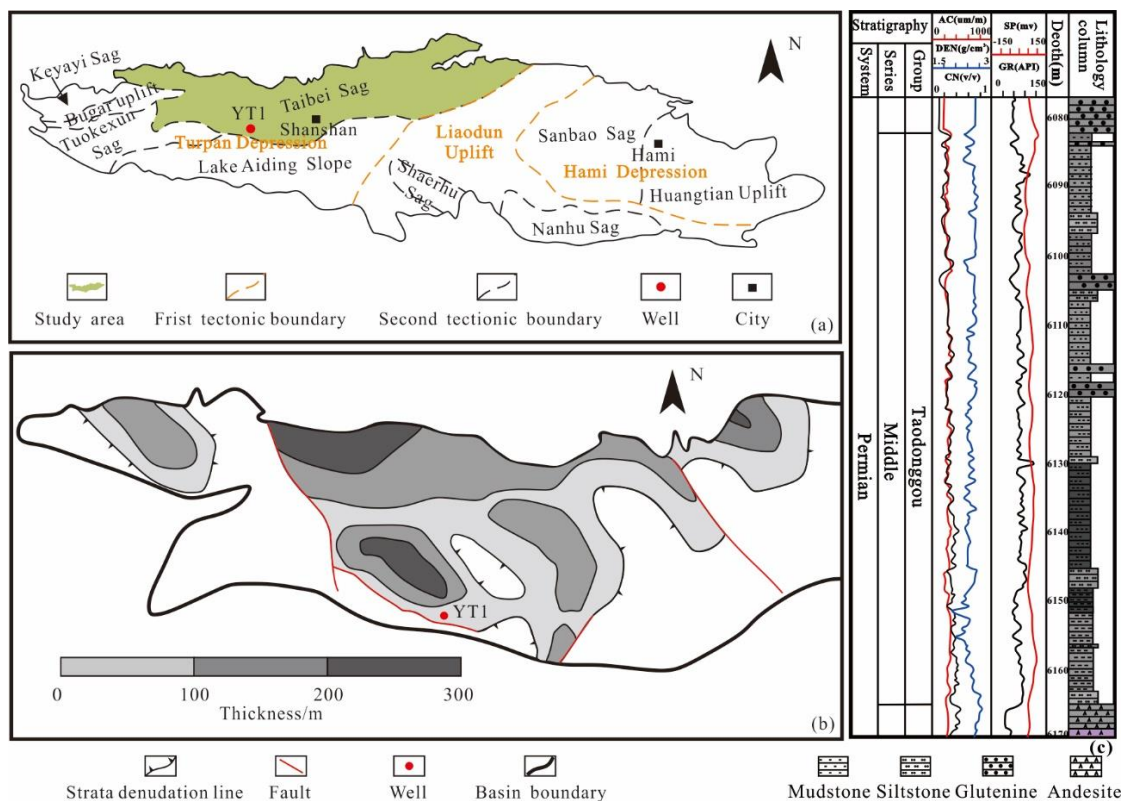
Fig.1 Geological overview of the study area (modified after Miao et al., 2021; Miao et al., 2022): (a) Geological background of Turpan-Hami

basin; (b) Thickness contour map of Taodonggou Group mudstone in Taibei sag; (c) YT1 stratum of Taodonggou Group

3 Samples and experiments

3.1 Samples

In this study, 16 mudstone samples were collected from well YT1, numbered YT1-1 to YT1-16 in order of depth. After

cleaning the samples, XRD, XRF and ICP-MS experiments were conducted.

3.2 Experiments

The XRD experiment was carried out in Hangzhou Yanqu Information Co., Ltd. The experimental instrument was the

Ultima VI XRD testing instrument of Japanese Neo Confucianism. In according with the Chinese industry standard SY/T

5163-2018, the mudstone was broken to a particle size of less than 200 meshes, and 2g samples were weighed to obtain XRD

images through Cu/Ka radiation at a scanning speed of 2°/min. The measurement angle range was $3° \leq 2\theta \leq 70 °$, and finally

quantitative interpretation is made with the software X'Pert Highscore Plus of Panalytic Company.

The XRF experiment was conducted in Hangzhou Yanqu Information Co., Ltd., and the experimental instrument was

PANalytical Axios tester from Panalytical. The mudstone was first crushed to a particle size of less than 200 meshes, then 10

g of the sample was weighed and calcined in a muffle furnace for 4 hours to get rid of organic matter and carbonates, weighed

and recorded the weight loss, and finally $Li_2B_4O_7$ was added, mixed evenly and made into glass bead, and the main element

105 concentration was tested.

106 The ICP-MS test was performed at Beijing Orient Smart, and the test instrument was an ELEMENT XR inductively

107 coupled plasma emission spectrometer manufactured by Thermo Fisher, Inc. Before analysis, the samples were ground to a

108 particle size of less than 40 μm. An appropriate amount of the sample was weighed and dissolved in HF (30%) and HNO3

109 (68%) at 190°C for 24 hours. After evaporating the excess solvent with deionized water, the solution was redissolved in 2 ml

110 of 6.5% HNO₃. Redissolve in 2 ml of 6 mol/L HNO₃ and then store at 150 ℃ for 48 hours. Subsequently, after evaporating

111 the solution, 1 ml of 6 mol/L HNO₃ evaporated solution was added to the sample.

112 **4 Results**

113 **4.1 Mineralogy**

114 The XRD test results of 16 samples from Well YT1 are shown in Table 1 and Figure 2. As can be seen from Table 1 and

115 Figure 2, Taodonggou Group mudstone are composed of clay, quartz, calcite, plagioclase, barite and K-feldspar, and some

116 samples contain siderite and pyrite. The content of clay is the highest (23.9% ～ 70.9%, mean 40.78%), followed by quartz

117 (17.2% ～ 59.2%, mean 34.69%), calcite (1% ～ 35.4%, mean 16.97%), barite (0% ～ 13.3%, mean 4.21%), plagioclase

118 (0% ～ 5.4%, mean 2.93%) and K-feldspar (0% ～ 2.3%, mean 0.9%).

119

Table.1 Mineral composition of Taodonggou Group mudstone in YT1 well

Samples	Depth/m	Minerals content (%)							
		Quartz	K-fledspar	Plagioclace	Calcite	Siderite	Pyrite	Barite	Clay
YT1-1	6084	29.4	0.7	1.8	23.7	/	/	13.3	31.1
YT1-2	6092	30.1	1.1	5.4	26.9	/	/	2.1	34.4
YT1-3	6102	41.9	/	2.5	18.1	/	/	3.2	34.3
YT1-4	6113	35.7	0.5	2.9	10.8	/	/	2.8	47.3
YT1-5	6122	40.5	0.1	2.7	19.4	/	/	4.6	32.7
YT1-6	6129	39.2	0.6	2.1	19.7	/	/	4	34.4
YT1-7	6136	27.9	0.3	0.8	42.8	/	/	4.3	23.9
YT1-8	6140	31.2	0.6	0.6	22.1	/	/	5.6	39.9
YT1-9	6143	34	0.4	0.2	14	/	/	4.5	46.9
YT1-10	6144.7	33.6	2.1	3.7	11.4	2.1	2.8	3.5	40.8
YT1-11	6145.3	37	/	3.7	10.6	1.4	/	2.1	45.2
YT1-12	6145.8	38.4	1.7	2.2	12.5	/	/	3.1	42.1
YT1-13	6147	37.9	/	/	1	/	1.4	1.2	58.5
YT1-14	6151	59.2	0.5	0.2	1.3	/	2.1	/	36.7
YT1-15	6154	21.8	0.8	0.8	1.8	/	/	3.9	70.9
YT1-16	6161	17.2	2.3	4.8	35.4	2	/	5	33.3

120 The mineral composition can be used to analyze the lithofacies type of mudstone, and different lithofacies types often

121 have different characteristics (Glaser et al., 2014). Previous scholars believed that mudstone types can be divided by the

122 ternary diagram of mineral composition. The three end elements of the ternary diagram are quartz + feldspar + mica (QFM),

123 calcite + dolomite + ankerite + siderite + magnesite (carbonate) and clay. The XRD results of 16 mudstone samples from Well

124 YT1 in the study area are put into the ternary map (Fig. 3). The results show that the data points of Taodonggou Group

125 mudstone in the study area are located in four areas, namely, mixed mudstone, silica-rich argillaceous mudstone, argillaceous

126 siliceous mudstone and mixed siliceous mudstone, and most of the points are mixed mudstone and argillaceous siliceous

127   mudstone areas, which indicates that Taodonggou Group mudstone can be divided into four types: mixed mudstone, silica-

128   rich argillaceous mudstone, argillaceous siliceous mudstone and mixed siliceous mudstone, and the main lithofacies are mixed

129   mudstone and argillaceous siliceous mudstone.
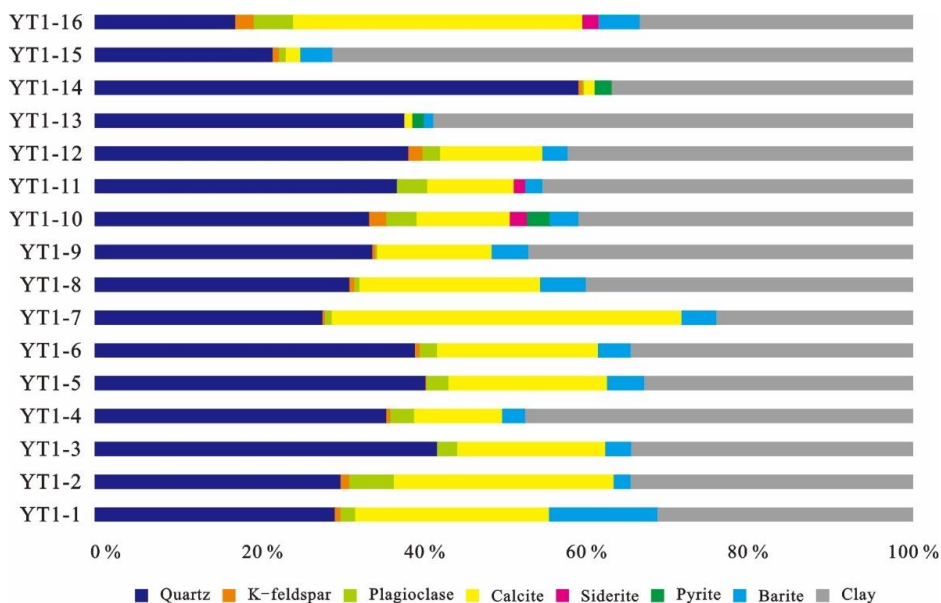
130

131   Fig.2 Mineral composition of Taodonggou group mudstone in YT1 well
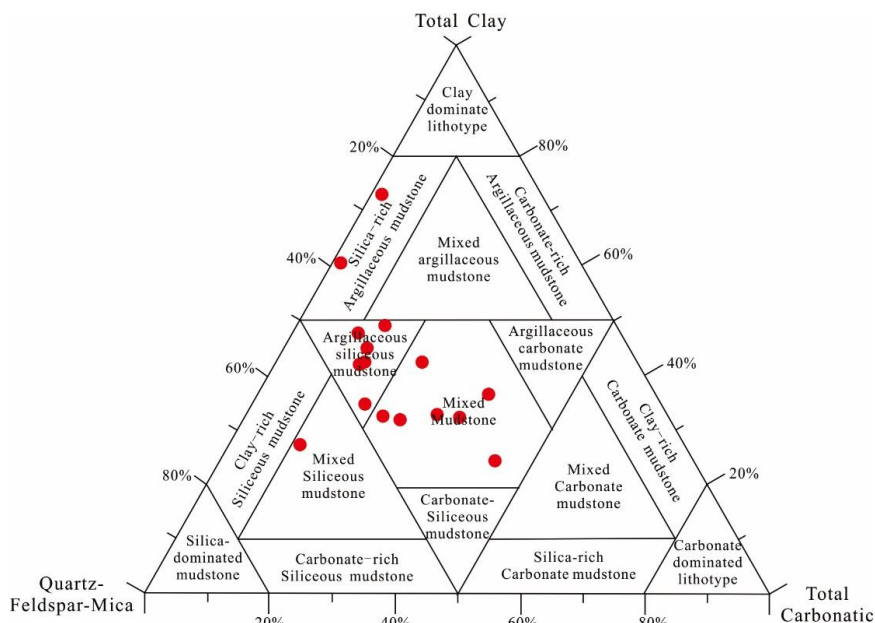
132

133   Fig.3 Lithofacies classification of Taodonggou Group mudstone in well YT1(modified from Glaser et al., 2014)

134   **4.2 Major element**

135   Table 2 shows the results of the major elements of 16 mudstone samples from Well YT1. From Table 2 we can see that

136   the major elements of Taodonggou Group mudstone are mainly SiO₂, Al₂O₃, Fe₂O₃, CaO and TiO₂. The highest content of

137   SiO₂ is from 43.11% to 70.11%, with an average value of 56.18%. Al₂O₃ content takes second place, accounting for 11.65%

138   to 25.75%, with an average value of 18.69%; The average content of another main element is less than 10%.

139

Table. 2 Major elements of Taodonggou Group mudstone in well YT1

| Samples | Depth/m | Content/% | | | | | | | | | | CIA | P/Ti | K₂O/Al₂O₃ |
		SiO₂	CaO	Al₂O₃	Fe₂O₃	K₂O	TiO₂	Na₂O	MgO	P₂O₅	MnO			
YT1-1	6084	43.79	19.05	11.65	5.32	3	1.35	1.15	1.1	0.9	0.3	68.71	0.49	0.26
YT1-2	6092	54.32	14.01	14.96	6.74	3.39	1.37	1.5	1.34	0.29	0.15	70.1	0.15	0.23
YT1-3	6102	56.63	14.36	11.66	5.42	3.38	1.24	1.23	1.36	0.16	0.19	66.63	0.09	0.29
YT1-4	6113	56.92	7.38	17.52	7.93	4.2	1.28	1.22	1.55	0.21	0.14	72.55	0.12	0.24
YT1-5	6122	51.15	12.62	15.25	7.55	3	1.33	1.2	1.15	0.3	0.34	73.85	0.17	0.20
YT1-6	6129	62.28	4.49	16.07	5.93	3.5	1.15	1.68	0.8	1.17	0.12	70.08	0.74	0.22
YT1-7	6136	52.44	9.31	16.57	8.63	2.54	1.5	1.55	0.66	0.37	0.34	74.57	0.18	0.15
YT1-8	6140	55.37	3.01	21.11	9.64	2.63	1.42	1.5	0.49	0.15	0.24	78.92	0.08	0.12
YT1-9	6143	60.24	2.76	21.27	8.73	1.92	1.76	0.84	0.36	0.23	0.22	85.5	0.09	0.09
YT1-10	6144.7	61.08	2.75	24.16	7.54	0.99	1.82	0.3	0.36	0.21	0.06	93.83	0.08	0.04
YT1-11	6145.3	61.02	2.94	25.39	6.84	0.59	1.84	0.31	0.36	0.26	0.06	95.45	0.10	0.02
YT1-12	6145.8	60.32	5.41	21.32	7.29	0.72	1.85	0.34	0.32	0.21	0.06	93.84	0.08	0.03
YT1-13	6147	60.76	1.83	25.75	7.68	0.68	1.95	0.19	0.35	0.25	0.05	96.07	0.09	0.03
YT1-14	6151	70.11	2.44	12.83	7.28	0.97	1.31	0.34	0.27	0.15	0.05	88.59	0.09	0.08
YT1-15	6154	49.39	1.92	25.41	12.25	2.84	2.87	1.57	0.46	0.15	0.06	80.97	0.04	0.11
YT1-16	6161	43.11	9.56	18.04	14.17	2.83	4.22	1.9	0.77	1.03	0.25	73.12	0.18	0.16

140   **4.3 Trace element**

141   The trace elements content of Taodonggou Group mudstone is shown in Table 3. Enrichment factor (EF) is an important

142   indicator of element enrichment (Taylor and Mclennan, 1985; Ross and Bustin, 2009). By comparing the trace element content

143   of Taodonggou Group mudstone with the global average shale (AS), the trace element enrichment factors in the study area

144   are calculated as follows:

145    $$X_{EF} = \frac{(X / Al)_{samples}}{(X / Al)_{AS}} \qquad (1)$$

146   Where X and Al represent the concentrations of elements X and Al (Taylor and Mclennan, 1985; Ross and Bustin, 2009).

147    $X_{EF} < 1$ represents the dilution concentration of element X relative to the standard composition, $X_{EF} > 1$ represents the relative

148   enrichment of element X compared to the AS concentration, $X_{EF} > 3$ represents the detectable autogenetic enrichment, and

149    $X_{EF} > 10$ is considered as an indicator of moderate to strong autogenetic enrichment (Taylor and Mclennan, 1985; Ross and

150   Bustin, 2009).

151   Figure 4 presents the enrichment factors of Taodonggou Group mudstone in the study area. It can be seen from Figure 4

152   that only Hf (1.29) is enriched in Taodonggou Group mudstone compared with AS, and other elements are not enriched.
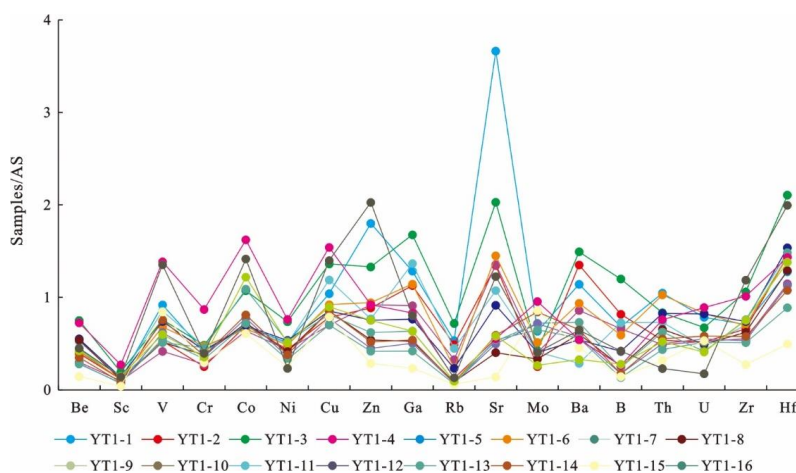
Figure 4 AS standardized multi-element diagrams of Taodonggou Group mudstone in the study area.

4.4 Rare earth element

The REE content of Taodonggou Group mudstone in the study area is shown in Table 4. According to Table 4, the $\sum$REE content of Taodonggou Group mudstone ranged from 43.247×10^{-6} to 257.997×10^{-6}, with an average value of 159.206×10^{-6}. The light rare earth element (LREE) content was the highest (mean value 133.45×10^{-6}), followed by medium rare earth element (MREE) (mean value 17.438×10^{-6}) and heavy rare earth element (HREE) (mean value 6.684×10^{-6}) in that order. After chondrite standardization (Taylor and Mclennan, 1985), Taodonggou Group mudstone shows a right dipping REE distribution pattern (Fig. 5), $(La/Yb)_N$ is 6.228~10.081, with an average value of 7.358.
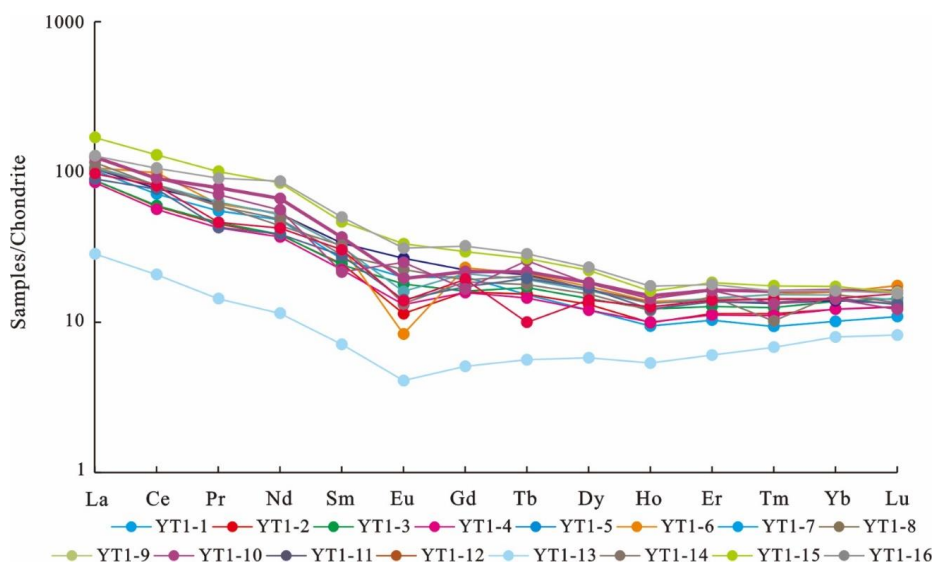
Figure 5. Standardized map of rare-earth element chondrite in mudstone of Taodonggou Group

Table.3 Characteristics of Trace elements in Taodonggou Group mudstone

Samples	YT1-1	YT1-2	YT1-3	YT1-4	YT1-5	YT1-6	YT1-7	YT1-8	YT1-9	YT1-10	YT1-11	YT1-12	YT1-13	YT1-14	YT1-15	YT1-16

	Depth/m	6084	6092	6102	6113	6122	6129	6136	6140	6143	6144.7	6145.3	6145.8	6147	6151	6154	6161
	Be	0.952	1.12	1.67	1	1.52	1.26	1.74	2.17	1.79	1.31	1.35	1.42	0.711	1.77	2.05	1.55
	Sc	9.02	11.9	15.5	11.7	13.6	13.1	15.6	16.2	21.2	11.4	13.2	12.3	7	24	26	17.6
	V	87.3	64.2	72	59.5	106	89.2	100	88.5	88.7	122.3	114.6	131.6	177	145	124	199
	Cr	27.4	21.2	31.8	27.3	40.1	43	40.1	45.1	54.8	48.5	47.6	44.5	43	63	51	40.2
	Co	9.46	12.4	14.9	13.3	11.9	12.6	13.7	18.2	27.6	22.3	21.7	20.6	18.7	24.8	36.9	30.4
	Ni	25.5	27.8	36.7	32.5	32.6	33.2	37.8	37.2	47.5	36.8	35.7	34.6	27.3	41.7	55.4	17.9
	Cu	34.2	33.1	44.8	34.6	51.2	41.8	39.9	50.8	48.9	52.6	50.3	51.4	57.3	55.8	64.4	71.2
	Zn	125	79	92.4	96.1	69.8	90.4	74.4	67.9	78.7	64.6	63.2	65.8	44.1	70.4	114	218
Content/(µg.g⁻¹)	Ga	17.81	20.1	23.3	19	24.8	21.9	15.1	13.2	16.1	14.5	12.7	13.7	7.14	12.7	19.2	17.3
	Rb	54.5	64.6	73.5	50.4	60	33.5	33.9	16	17.9	15.6	14.6	14.6	13.6	14.2	21	20.7
	Sr	758	357	420	422	291	414	269	151	199	214	244	224	63.9	126	263	393
	Mo	1.29	0.661	0.866	1.24	1.09	1.44	1.17	1.23	2.68	3.02	2.88	3.14	3.86	2.14	1.18	1.28
	Ba	483.83	735.7	633	547.28	159.24	547.66	326.49	465.2	565	503	516	505	427	254	303.56	424.35
	B	46.31	71.3	81.4	67.4	64.5	55.4	60.2	41.3	49.6	44.6	52.6	41.4	41.5	39.7	56.2	54.1
	Th	9.16	6.03	7.31	6.43	8.38	12.4	10.3	10.4	10	9.12	8.33	8.86	6.17	7.32	9.96	3.13
	U	2.13	1.8	1.83	2.14	1.66	3.1	3.17	2.43	2.06	3.1	3.06	2.89	3.2	2.66	2.42	0.73
	Zr	82.7	99.3	124	97.1	107	112	123	132	162	128.8	130.2	123.6	70.8	130.4	192	215
	Hf	2.6	3.77	4.29	3.51	3.87	4.03	4.45	4.76	5.52	4.76	3.94	4.01	2.23	3.21	6.13	6.29
Sr/Ba		1.57	0.49	0.66	0.77	1.83	0.76	0.82	0.32	0.35	0.43	0.47	0.44	0.15	0.5	0.87	0.93
Ga/Rb		0.33	0.31	0.32	0.38	0.41	0.65	0.45	0.83	0.9	0.93	0.87	0.94	0.53	0.89	0.91	0.84
B/Ga		2.6	3.55	3.49	3.55	2.6	2.53	3.99	3.13	3.08	3.08	4.14	3.02	5.81	3.13	2.93	3.13
Rb/K/(10⁻⁴)		21.87	22.94	26.18	14.45	24.08	11.52	16.07	7.32	11.22	18.97	29.79	24.41	24.08	17.63	8.9	8.81
V/Cr		3.19	3.03	2.26	2.18	2.64	2.07	2.49	1.96	1.62	2.52	2.41	2.96	4.12	2.3	2.43	4.95
V/(V+Ni)		0.77	0.7	0.66	0.65	0.76	0.73	0.73	0.7	0.65	0.77	0.76	0.79	0.87	0.78	0.69	0.92

165

Table 4 Characteristics of REE in Taodonggou Group mudstone

Samples	Depth/m	La	Ce	Pr	Nd	Sm	Eu	Gd	Tb	Dy	Ho	Er	Tm	Yb	Lu	∑REE	LREE	MREE	HREE	(La/Yb)$_N$
YT1-1	6084.00	31.70	57.70	6.73	28.84	5.16	1.49	5.19	0.72	3.87	0.60	2.10	0.32	2.13	0.35	146.95	124.93	17.07	4.946	10.081
YT1-2	6092.00	27.30	47.80	5.51	22.99	4.79	0.83	4.13	0.71	4.25	0.71	2.40	0.37	2.56	0.40	124.69	103.51	15.44	5.738	7.190
YT1-3	6102.00	27.30	48.30	5.62	23.10	4.71	1.32	4.17	0.80	4.63	0.88	2.68	0.41	2.89	0.46	127.27	104.32	16.51	6.440	6.369
YT1-4	6113.00	26.40	45.60	5.20	22.20	4.37	0.96	4.09	0.78	3.88	0.82	2.35	0.36	2.66	0.40	119.78	99.400	14.705	5.678	6.953
YT1-5	6122.00	32.60	62.80	7.61	31.70	6.56	1.96	5.77	0.98	5.35	0.97	2.89	0.43	3.29	0.42	162.971	134.71	21.590	6.671	7.527
YT1-6	6129.00	33.10	80.10	7.48	31.70	6.19	0.62	5.98	0.98	5.59	0.91	3.00	0.50	3.38	0.56	180.108	152.38	20.348	7.383	6.742
YT1-7	6136.00	33.50	66.40	7.70	31.20	6.19	1.18	5.46	0.91	5.24	0.95	3.09	0.49	3.14	0.45	165.91	138.80	19.936	7.178	7.102
YT1-8	6140.00	35.90	65.80	7.23	29.20	5.47	1.66	4.95	0.95	5.36	0.95	2.97	0.47	3.06	0.42	164.346	138.13	19.346	6.872	8.041
YT1-9	6143.00	39.00	73.40	9.60	40.00	7.18	1.44	5.64	1.02	5.91	1.08	3.45	0.52	3.41	0.51	192.169	162.00	22.270	7.899	7.711
YT1-10	6144.70	32.60	66.43	7.34	26.40	6.31	0.98	4.82	0.84	4.97	0.86	3.12	0.43	3.21	0.43	158.646	132.77	18.130	7.096	6.847
YT1-11	6145.30	27.90	62.23	5.23	23.20	5.42	1.04	4.46	0.82	5.41	0.88	2.88	0.42	3.23	0.42	143.453	118.56	17.880	6.763	6.228
YT1-12	6145.80	30.20	65.60	5.64	25.40	5.93	1.02	5.01	0.87	4.54	0.81	2.94	0.46	3.01	0.50	151.631	126.84	5.531	6.911	6.764
YT1-13	6147.00	8.84	16.80	1.75	6.90	1.39	0.30	1.37	0.27	1.89	0.37	1.27	0.27	1.62	0.26	43.247	34.290	5.531	3.426	3.569
YT1-14	6151.00	39.40	73.60	8.64	33.60	4.20	1.80	4.31	1.23	5.83	1.03	3.43	0.42	2.92	0.39	180.91	155.242	5.531	7.222	8.914
YT1-15	6154.00	52.60	105.00	12.30	50.80	9.09	2.45	7.65	1.24	7.14	1.16	3.86	0.57	3.60	0.51	257.997	220.70	28.74	8.557	9.796
YT1-16	6161.00	39.70	85.70	11.10	52.10	9.76	2.29	8.33	1.34	7.47	1.25	3.75	0.52	3.39	0.50	227.206	188.60	30.44	8.166	7.895

166   LREE = La + Ce + Pr + Nd; MREE = Sm + Eu + Gd + Tb + Dy + Ho; HREE = Er + Tm + Yb + Lu; (La/Yb)$_N$ = (La/Yb)/(La/Yb)$_{chondrite}$

167 **5 Discussion**

168   Mineral composition and element geochemical characteristics are one of the important means to analyze the type of

169   parent rock, sedimentary environment and tectonic setting. Therefore, this study provides mineralogy and element

170   geochemical characteristics to analyze the parent rock type, sedimentary environment and tectonic setting source area of

171   Taodonggou Group mudstone in Taibei Sag, Turpan-Hami Basin.

172   5.1 Paleoclimate and weathering

173   The paleoclimate not only affects the weathering degree of the parent rock, but also affects the transport distance of

174   sedimentary debris and the transport of nutrients (Zhang et al., 2005). There are many evaluation indexes of paleoclimate,

175   such as chemical alteration index (CIA) and climate index (C). It is generally believed that when CIA=50~65 and C < 0.2, it

176   reflects that the sedimentary system is in a dry and cold climate under the background of lower of degree of chemical

177   weathering; when CIA=65~85 and 0.2 < C < 0.8, it indicates that the sedimentary system is in a warm and humid climate

178   under the background of middle of degree of chemical weathering; when CIA=85~100 and C > 0.8, it reflects the humid and

179   hot climate under the background of high of degree of chemical weathering (Zhang et al., 2019; Nesbitt and Nesbitt, 1984).

180   The calculation formula of CIA and C is as follows:

181    $$CIA = \frac{Al_2O_3 \times 100}{Al_2O_3 + Na_2O + CaO^* + K_2O} \qquad (2)$$

182    $$C = \frac{Fe + Mn + Cr + Ni + V + Co}{Ca + Mg + Sr + Ba + K + Na} \qquad (3)$$

183   In formula (2), CaO * only refers to CaO in silicate minerals. Due to the lack of direct measurement means, it is often

184   calculated indirectly by the content of P_2O_5, namely:

185    $$CaO^* = mol(CaO) - \frac{10}{3} mol(P_2O_5) \qquad (4)$$

186   Where, mol(CaO) and mol(P_2O_5) are the mole numbers of CaO and P_2O_5, where when mol (Na_2O) ≤ mol (Cao *), mol

187   (Ca0 *) = mol (Na_2O); on the contrary, when mol(Na_2O) > mol(CaO^*), mol(CaO^*)=mol(CaO) (Nesbitt and Young, 1984).

188   The CIA values of the Taodonggou Group mudstone in the study area were calculated based on Equation (2) and Equation

189   (3), ranging from 68.71 to 96.97, with a mean value of 80.17. The climate index (C) is 0.22 ～ 2.42 (average = 1.01). The

190   overall paleoclimate was warm-humid and hot (Fig. 7a). According to Table 2, the relationship between CIA value and depth

191   is analyzed, and it is found that the CIA value first increases and then decreases with depth, indicating that Taodonggou Group

192   mudstone was deposited in a warm, humid and hot paleoclimate, and can be divided into three stages.

193   In addition, the cross plot of Ga/Rb and K_2O/Al_2O_3 can also be used to analyze the paleoclimate characteristics during

194   the formation of sedimentary rocks (Lerman and Baccini, 1987; Liu and Zhou, 2007). As shown in the cross plot of Ga/Rb

195   and K_2O/Al_2O_3 (Fig. 7b), almost all points are in the warm/wet area, which indicates that Taodonggou Group mudstone was

196   deposited in a warm and humid paleoclimate.

197   Based on the above analysis, Taodonggou Group mudstone in the study area were deposited in a warm, humid and hot

198   paleoclimate. This result is consistent with Miao's indicator result using the biomarker parameter CPI (Miao et al., 2021),

199   indicating that the biomarker parameter CPI can be used to explain the paleoclimate change characteristics of hydrocarbon

200   source rocks with Ro ≤ 1.49.
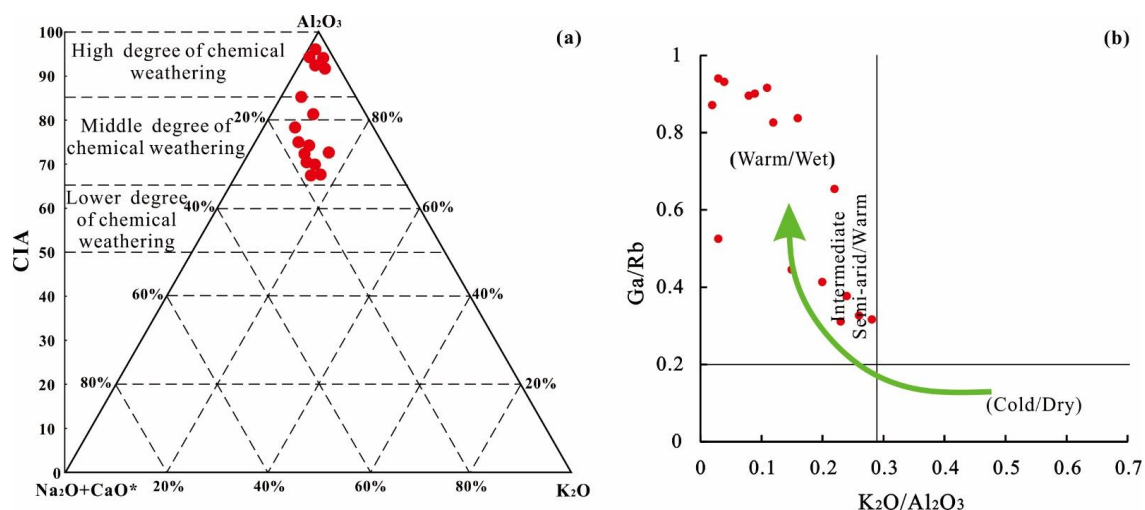
202   Figure.6 Paleoclimate index of Taodonggou Group: (a) CIA Characteristics of Taodonggou Group mudstone (modified from Nesbitt and Young,

203   1984); (b) cross plot of K_2O/Al_2O_3 and Ga/Rb (modified from Roy and Roser, 2013)

204   **5.2 Provenance**

205   5.2.1 Lithology of parent rock

206   Previous studies have found that the chemical composition of the rocks in the sedimentary area and the parent rock in

207   the provenance area has a strong affinity, and the type of parent rock will directly affect the element geochemical

208   characteristics of the sediment (Tribovillard et al., 2006; Shi et al., 2021; McLennan et al., 1993; Basu et al., 2016; Hu et al.,

209   2021; Floyd and Leveridge, 1987; Wronkiewicz and Condie, 1987). Generally speaking, the transport of sediment from the

210   source area to the sedimentary area goes through multiple complex processes such as mechanical transport and chemical

211   action, and hence it is necessary to analyze the impact of sediment sorting and recycling on each chemical component when

212   identifying the source Previous studies have shown that trace elements Zr, Th and Sc are relatively stable in geological

213   processes such as weathering, transportation and sorting, and are not easily lost, which can be used as one of the indicators

214   for parent rock identification(Floyd and Leveridge, 1987; Wronkiewicz and Condie, 1987). According to Th/Sc and Zr/Sc

215   intersection diagram of Taodonggou Group mudstone (Fig. 7a), Taodonggou Group mudstone is close to andesite and felsic

216   volcanic rock of the upper crust, and its composition is controlled by the composition of felsic parent rock, and has not

217   undergone sediment sorting and recycling.

218   In addition, REE and trace elements in mudstone from different parent rocks are obviously different, so the ratio of REE

219   to trace elements can be used to analyze the type of parent rock, and most common ones are La/Sc, La/Co, Th/Sc, Th/Co and

220   Cr/Th (Basu et al., 2016; Hu et al., 2021; Floyd and Leveridge, 1987; Wronkiewicz and Condie, 1987; Allègre and Minster,

221   1978). Based on the Hf and La/Th intersection diagram (Fig. 7b) and the La/Sc and Co/Th intersection diagram (Fig. 7c), we

222   can see that Taodonggou Group mudstone have both andesitic island-arc sources and felsic volcanic sources. It can be seen

223   from the cross plot of TiO_2 and Zr (Fig. 7d) that Taodonggou Group mudstone have a source of intermediate igneous rocks

224   and felsic igneous rocks. As can be seen from the cross plot of La/Yb and Σ REE (Fig. 7e), almost all data points are located

225   in the sedimentary rock area, alkali basalt and granite area.

226   In summary, the parent rocks of Taodonggou Group mudstone are andesitic and feldspathic volcanic rocks, with weak

227   sedimentary sorting and recirculation, and the material source information is well-preserved.
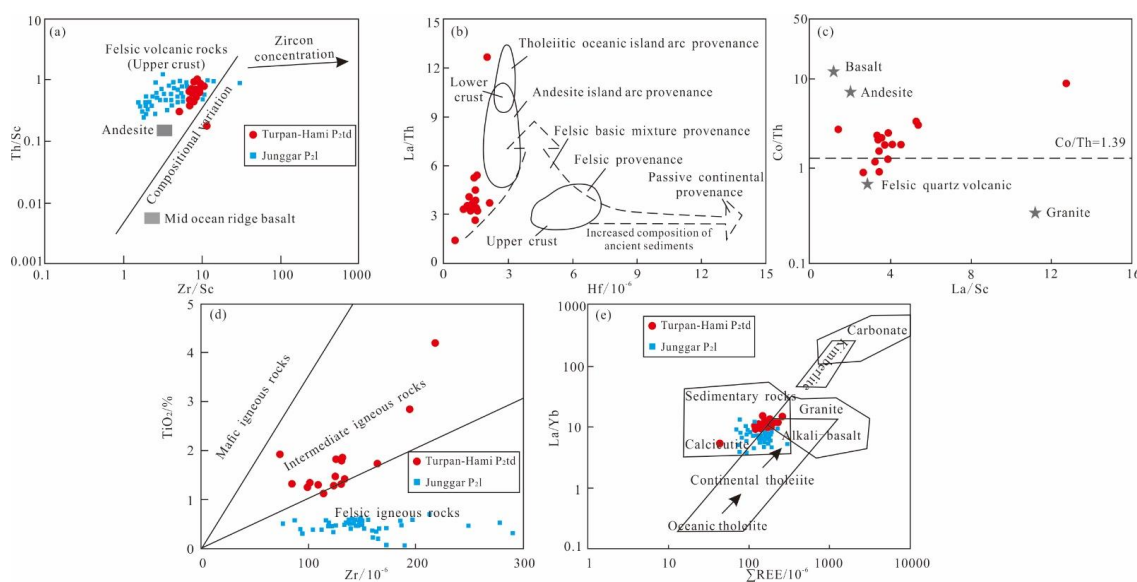
228

229   Figure.7 Parent rock type of Taodonggou Group in YT1 well (Data of Lucaogou Formation in Junggar Basin are from Li et al., 2020): (a) Th/Sc

230   and Zr/Sc intersection diagram(modified after Floyd and Leveridge, 1987); (b) La/Th and Hf intersection diagram(modified after Floyd and

231   Leveridge, 1987); (c) Co/Th and La/Sc intersection diagram(modified after Wronkiewicz and Condie, 1987); (d) TiO_2 and Zr intersection

232   diagram; (e) La/Yb and ∑REE intersection diagram (modified after Allègre and Minster, 1978)

233   5.2.2 Location of Parent Rock

234   There is a great controversy about the provenance location of the Middle Permian in Turpan-Hami (Shao et al., 2001;

235   Jiang et al., 2015; Wang et al., 2019; Zhao et al., 2020; Song et al., 2018; Wang et al., 2018; Tang et al, 2014). Shao et al.

236   (1999) believed that the provenance of the Permian was mainly from the Jueluotage Mountain in the south of the Turpan-

237   Hami Basin, Song et al. (2018) considered that it came from Bogda area, Zhao et al. (2020) believed that the provenance of

238   the Permian in the Turpan-Hami Basin was consistent with that in Junggar, and originated from the Kelameili Mountain and

239   the Northern Tianshan. Summarizing the previous research results, it is found that the main controversial point is the time of

240   the first uplift of Bogda Mountain.

241   At present, there are many opinions about the time of Bogda Mountains uplift. They think that the initial uplift of Bogda

242 Mountains occurred in Early Permian (Carroll et al., 1990; Shu et al., 2011; Wang et al., 2018; Li et al., 2022), Middle Permian

243 (Zhang et al., 2006; Liu et al., 2018; Wang et al., 2018), Late Permian-Early Triassic (Zhao et al., 2020; Guo et al., 2006;

244 Wang, 1996; Sun and Liu, 2009; Tang et al., 2014; Wang et al., 2018), Middle Triassic (Guo et al., 2006), Early Jurassic

245 (Green et al., 2005; Liu et al., 2017; Ji et al., 2018) and Late Jurassic (Yang et al., 2015). If the initial uplift of the Bogda

246 Mountains was after the middle Permian, the parent rock types of the Taodonggou Group (P$_2$td) mudstone in the Turpan-Hami

247 Basin and the Luchaogou Formation (P$_2$l) mudstone in the Junggar Basin should be the same.

248 We have counted the element geochemical characteristics of Luchaogou Formation (P$_2$l) in the Junggar Basin (Li et al.,

249 2020), and found that the parent rock type of P$_2$l mudstone in the Junggar Basin is greatly different from that of P$_2$td, which

250 is felsic volcanic rock (Fig. 7). Therefore, the initial uplift of Bogda Mountain should Late Permian-Early Triassic in the Early

251 Permian or Middle Permian. This is consistent with li et al. (2022) and Wang et al. (2018) who inferred the uplift of Bogda

252 Mountain at 289.8 Ma-265.7 Ma. Shao et al. (2001) believed that the sandstone of the Daheyan Formation in Turpan-Hami

253 Basin has a good affinity with the Early Permian and Carboniferous, so the provenance direction of the sandstone of Daheyan

254 Formation is consistent with that of the Early Permian, and they all come from the Jueluotage Mountain. However, the

255 paleocurrent direction of the Early Permian in Xinjiang is southeast (Zhang et al., 2005; Li et al., 2007; Wang et al., 2019),

256 and the provenance area is located in the north of Bogda area. Zhao et al. (2020) calculated the U-Pb dating results of 5250

257 zircons in the Tianshan and believed that the provenance of the Turpan-Hami Basin and the Junggar Basin both came from

258 the northern Tianshan and the Kelameili Mountain, which is also consistent with the ancient ocean current direction in the

259 Early Permian (Zhang et al., 2005; Li et al., 2007; Wang et al., 2019; Fig. 8a). Consequently, the first uplift of Bogda Mountain

260 should have occurred in the Early Permian, but it was not exposed in the early Middle Permian and it still received

261 sedimentation. In the middle Middle Permian, the exposed water began to be denuded, becoming the source area of the

262 Turpan-Hami Basin (Wang et al., 2018).

263 Based on the above analysis, in the early Middle Permian, although Bogda Mountain in the north of Turpan-Hami Basin

264 was uplifted due to orogeny, it did not emerge from the water surface, and it still accepted the provenance of North Tianshan

265 and Kelameili Mountain. At this time, there was a NE trending ancient ocean current (Carrollet al., 1995; Obrist-Farnert et

266 al., 2015; Zhao et al., 2020), so Jueluotage Mountain, which has been uplifted in the south of Turpan-Hami Basin, became a

267 secondary provenance area (Shao et al., 1999; Fig. 8b). With the continuous uplift of Bogda Mountain, the sedimentary center

268 of Turpan-Hami Basin gradually shifted to Taibei Sag, and the provenance area of Turpan-Hami Basin changed to Bogda

269 Mountain and Jueluotage Mountain (Fig. 8c).
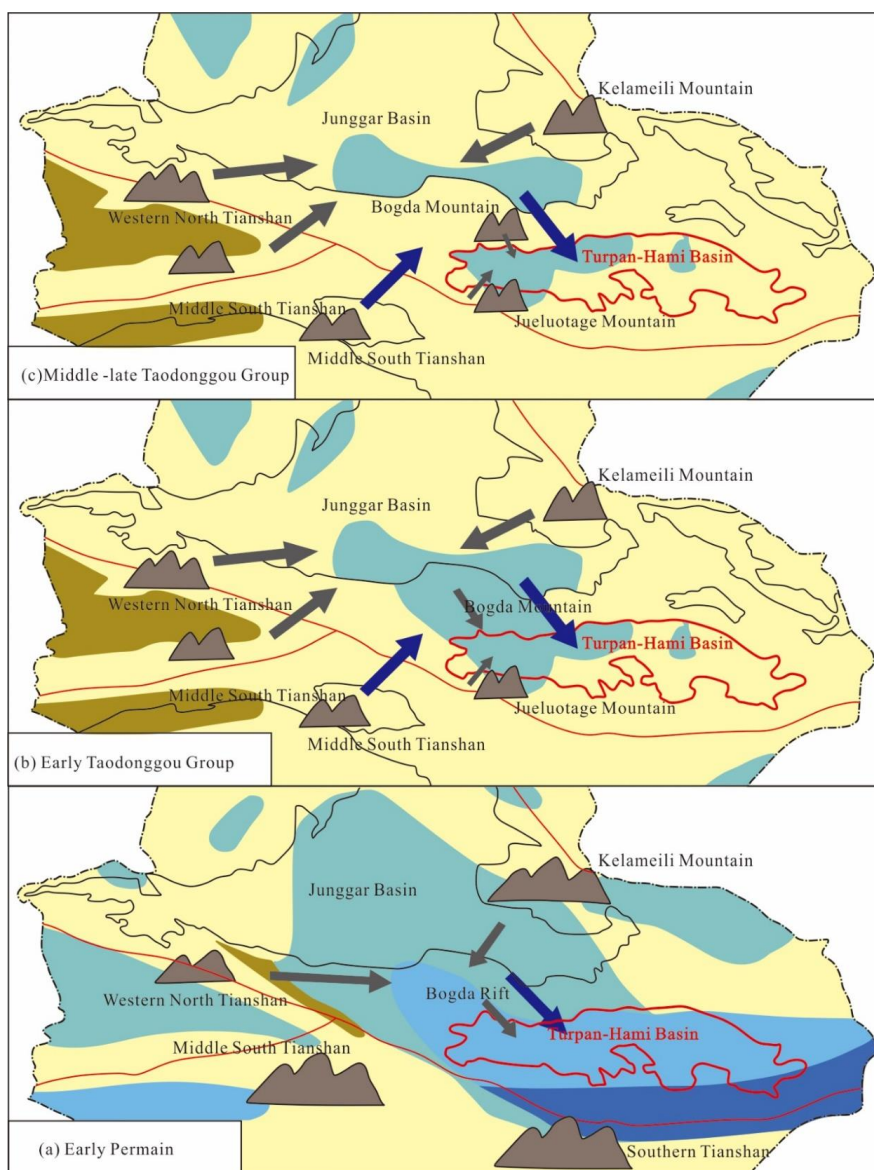
Figure. 8 Provenance location from Early Permian to Middle Permian in Tianshan area (modified after Zhao et al., 2020):

(a) Early Permian; (b) Early of Taodonggou Group; (c) Middle to later of Taodonggou Group

5.3 Paleosedimentary environment

5.3.1 Paleo-redox conditions

Redox environments are critical to the preservation of organic matter in sedimentary rocks, and sensitive elements such as Co, Mo, U, Th, V, Ni and Cr are commonly used to identify redox conditions in ancient water bodies. Previous evidence suggests that U/Th < 0.75, V/Cr < 2 and V/(V+Ni) < 0.45 represent an oxic conditions, 0.75 < U/Th < 1.25, 2 < V/Cr < 4.25 and 0.45 < V/(V+Ni) < 0.84 represent a dyoxic conditions, U/Th < 1.25, V/Cr < 4.25 or V/(V+Ni) < 0.84 represent an anoxic

279   condition (Hatch and Leventhal, 1992; Rosenthal et al., 1995; Tribovillard et al, 2006; Tribovillard et al, 2012). There is no

280   significant correlation between V, U and Th and Al_2O_3 contents in the Taodonggou Group mudstone samples, indicating that

281   V, U and Th contents in Taodonggou Group mudstone are mainly controlled by authigenic deposition under redox conditions

282   (Tribovillard et al, 1994). The U/Th, V/Cr and V/(V+Ni) of the Taodonggou Group mudstone range from 0.21 to 0.52 (mean

283   = 0.29), 1.62 to 4.95 (mean = 2.7) and 0.65 to 0.92 (mean = 0.75), respectively. In the light of U/Th, Taodonggou Group

284   mudstone were deposited in an oxic environment, and according to V/Cr and V/(V+Ni), Taodong Group mudstone were

285   deposited in a dyoxic environment. This is because U/Th cannot accurately identify the redox environment of the sediments

286   under highly weathered conditions (Cao et al., 2021), so V/Cr and V/(V+Ni) were used in this study to identify the redox

287   environment of Taodonggou Group mudstone. The cross plot of V/Cr and V/(V+Ni) shows (Fig. 9) that Taodonggou Group

288   mudstone were deposited in a dyoxic environment.

289
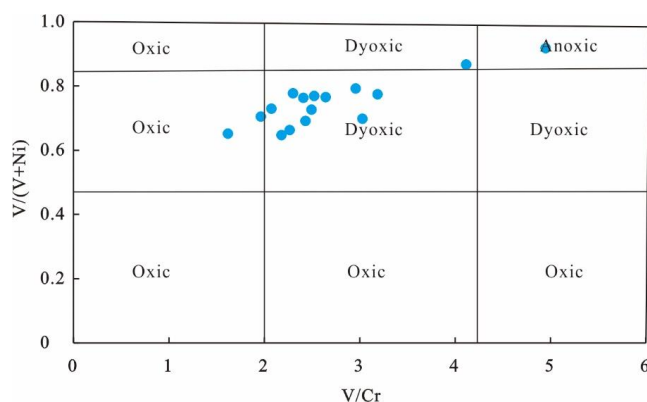
290   Figure.9 Cross plot of V/Cr and V/(V+Ni)

291   5.3.2 Paleosalinity

292   Paleosalinity is an important indicator of water body paleoenvironment. The level of paleosalinity affects the

293   stratification of the sedimentary water body and the development of plankton, thereby affecting the paleoproductivity and the

294   enrichment of organic matter in the sedimentary environment (Thorpe et al., 2012; Wang et al., 2021; Shi et al., 2021). There

295   is a consensus among previous studies that Sr/Ba and B/Ga can represent the change of paleosalinity. It is generally believed

296   that Sr/Ba<0.5 or B/Ga<3 represents fresh water, 0.5<Sr/Ba<1 or 3<B/Ga<6 means brackish water, and Sr/Ba>1 or B/Ga>6

297   represents saline water. The correlation between Sr and CaO of Taodonggou Group mudstone in the study area is not obvious

298   (R^2=0.17), Sr/Ba of Taodonggou Group mudstone in the study area range from 0.32 to 1.83, with an average value of 0.71,

299   and the B/Ga is 2.53 ～ 5.81 (average = 3.36), indicating that Taodonggou Group mudstone were deposited in freshwater and

300   brackish water environments (Fig. 10a).

301   In addition, Ca/(Ca+Fe) is a reliable indicator for evaluating the salinity of lake waters (Wang et al.,2021). The Ca/(Ca+Fe)

302   distribution of Taodonggou Group mudstone in the study area ranges from 0.14 to 0.78, with a mean value of 0.42. The Sr/Ba

303   and Ca/(Ca+Fe) intersection diagram (Fig. 10b) shows that Taodonggou Group mudstone were deposited in freshwater and

304   brackish water environments, which is in accord with the Sr/Ba and B/Ga intersection diagram.
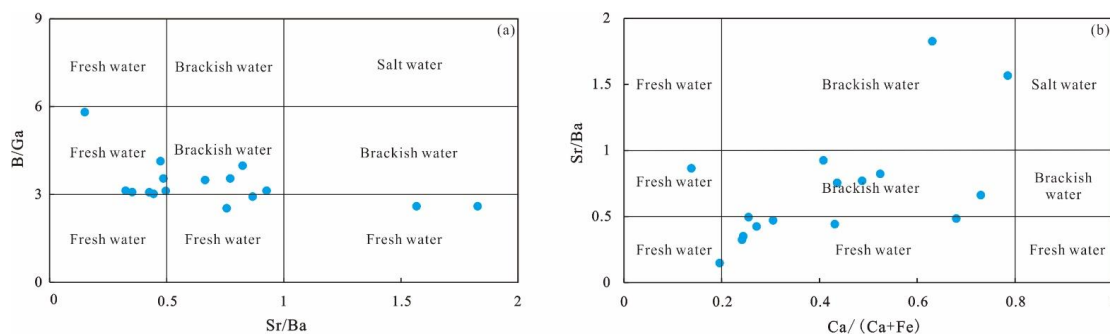
305

306   Figure.10 Cross plot of B/Ga and Sr/Ba (a) and cross plot of Ca/(Ca+Fe) and Sr/Ba (b)

307   5.3.3 Paleobathymetry

308   Previous studies have shown that some elements in the sedimentation process have obvious differences with the change

309   of offshore distance. These elements can be used to judge thewater depth variation in the sedimentation period. The commonly

310   used indicators are Zr/Al, Rb/K and MnO content (Xiong and Xiao, 2011; Herkat et al., 2013). It is now believed that the

311   lower the Zr / Al ratio or the higher the Rb / K ratio, the further offshore and the deeper the water (Xiong and Xiao, 2011;

312   Herkat et al., 2013). Zr/Al of Taodonggou Group mudstone is $5.19 \times 10^{-4} \sim 22.51 \times 10^{-4}$ (average = 13.44×10^{-4}), showing a

313   trend of first decreasing and then increasing with the depth, Rb/K ranges from 7.32×10^{-4} to 29.79×10^{-4} (mean 19.02×10^{-4}

314   ^{4}), with large fluctuations with depth of burial. The high-value area of Rb/K is basically consistent with the low-value area of

315   Zr/Al, which indicates that the ancient water depth during the Taodonggou Group mudstone deposition process has a trend of

316   first decreasing and then increasing.

317   For the content of MnO, it is generally believed that < 0.00094% is a shore lake, 0.00094 % ~ 0.0075 % is shallow lake,

318   0.0075 % ~ 0.051 % is an intermediate depth lake, and > 0.051% is a deep lake (Herkat et al., 2013). According to Table 2,

319   MnO of Taodonggou Group mudstone is 0.05% ～ 0.30%, with an average of 0.16 %, which indicates that the Taodonggou

320   Group mudstone are mainly deposited in intermediate depth - deep lake sedimentary environment.

321   5.3.4 Terrigenous detritus input

322   Ti, Si and Al are relatively stable during diagenesis and are usually used as indicators of debris flux input (Algeo and

323   Maynard, 2004; Maravelis et al., 2021). Generally, Ti in sediments comes from ilmenite ($FeTiO_3$) or rutile (TiO_2), while Al

324   can exist in feldspar, clay minerals and other aluminum silicate minerals (Algeo and Maynard, 2004). Compared with Ti and

325   Al, Si comes from many sources, including both biological origin and hydrothermal and terrigenous clastic input (Kidder and

326   Erwin, 2001). Therefore, when using SiO_2 as the evaluation index for terrigenous clastic input, its source needs to be analyzed.

327   The correlation of Al_2O_3 and TiO_2 with SiO_2 in the Well YT1 of the study area is not obvious, which indicates that their

328   sources are more complex and not dominated by terrestrial debris sources (Fig. 11). Therefore, Al_2O_3 and TiO_2 are used in

329   this study to indicate the terrestrial debris input during the deposition of the Taodonggou Group mudstone.

330   The Al$_2$O$_3$ content of YT1 wells is higher, ranging from 11.65 % to 25.75 %, with an average value of 18.69 %; the TiO$_2$

331   is 1.15 % ～ 4.22 %(average = 1.77 %). As can be seen from Table 2, the Al$_2$O$_3$ content of Well YT1 fluctuates more with

332   depth, and the overall trend is increasing first and then decreasing with depth, while the TiO$_2$ fluctuates less with depth, and

333   on the whole, the trend is increasing with depth. Combined with the results of paleoclimate analysis in the study area, it is

334   found that the terrestrial debris input during the deposition of the Taodonggou Group strata has the characteristics of increasing

335   first and then decreasing.
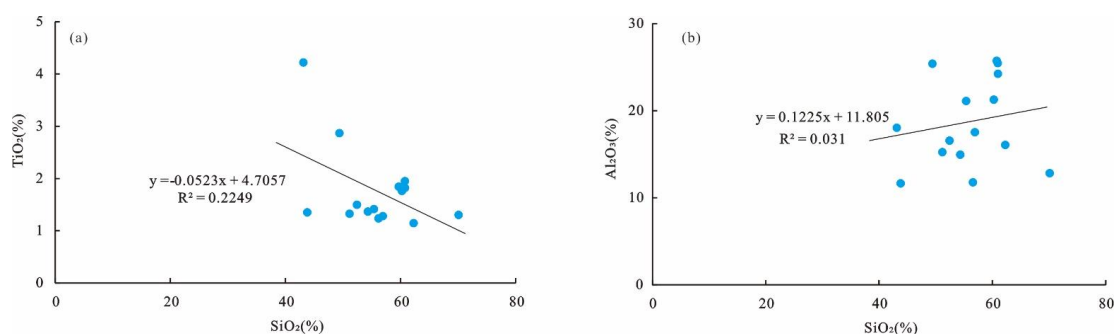
336

337   Figure.11 Intersection diagram of TiO$_2$ and SiO$_2$ (a) and intersection diagram of Al$_2$O$_3$ and SiO$_2$ (b)

338   5.3.5 Paleoproductivity

339   Paleoproductivity determines the quantity of original organic matter in sedimentary rocks (Wei et al., 2012; Algeo and

340   Ingall, 2007; Ross and Bustin, 2009; Schoepfer et al., 2015). The elements P, Si, Ba, Zn and Cu are indicators of the magnitude

341   of paleoproductivity, but they all have a certain range of application, for example, only the biogenic part of Si and Ba can

342   represent the productivity, and Zn can only represent the productivity change in the sulfide reduction environment (Wei et al.,

343   2012; Algeo and Ingall, 2007).

344   P is not only a key nutrient element in biological metabolism, but also an important component of many organisms, so it

345   can also be used to characterize biological productivity (Kidder and Erwin, 2001). In order to eliminate the influence of

346   terrigenous detritus, P/Ti or P/Al is usually used to reflect biological productivity. The P/Ti of Taodonggou Group mudstone

347   in the study area ranges from 0.04 to 0.74 %, with an average value of 0.17 % and an overall low productivity. As shown in

348   Table 2, the relationship between P/Ti and depth was analyzed, and the results showed that the paleontological productivity

349   tended to increase and then decrease with depth.

350   In addition, Cu also an important nutrient, unlike P, is generally indicative of productivity including the sum of primary

351   productivity and productivity from terrestrial inputs (Schoepfer et al., 2015). For the purpose of eliminating the dilution

352   interference of terrigenous detritus, Cu/Ti is used as an indicator to evaluate the paleoproductivity in this study. The

353   distribution range of Cu/Ti of Taodonggou Group mudstone in the study area is from 0.55 to 1.96 with an average value of

354   1.02, and gradually decreases with depth, indicating a gradual increase in palaeoproductivity during the deposition of

355   Taodonggou Group mudstone.

356   5.3.6 Deposition rate

357   The deposition rate is one of the parameters characterizing the magnitude of the dilution effect during deposition and is

358   commonly characterized by $(La/Yb)_N$. It is generally believed that the difference between LREE and HREE migration is not

359   significant when the sedimentation rate of the lake basin is faster and the $(La/Yb)_N$ value is close to 1. Conversely, when the

360     $(La/Yb)_N$ value is greater or less than 1, it indicates that the sedimentation rate of the lake basin is slower (Wang et al., 2021;

361   Cao et al., 2018). The $(La/Yb)_N$ of Taodonggou Group mudstone are 6.228~10.081, with an average value of 7.358 in the

362   study area, which is much greater than 1. This indicates that the Taodonggou Group mudstone have a slower deposition rate.

363   5.3.7 Hydrothermal activity

364   The study area has been extremely volcanically active since the Carboniferous to the Permian, with extensive volcanic

365   deposits in the Middle Permian Taodongou Group, the Lower Permian Yierxitu Formation, and the Carboniferous in the study

366   area. In order to explore whether a hydrothermal activity is involved in the Middle Permian sedimentation, the Zn-Ni-Co

367   ternary diagram and (Cu+Co+Ni) × 10-Fe-Mn ternary diagram are applied in this study (Xu et al., 2022; You et al., 2019).

368   Based on the Zn-Ni-Co ternary diagram (Fig. 12a), some data points of the Taodonggou Group mudstone are distributed in

369   the hydrothermal sedimentary zone, and based on the (Cu+Co+Ni)×10-Fe-Mn ternary diagram (Fig. 12b), all data points of

370   the samples fall in the hydrothermal sediments zone and Red Sea hydrothermal sediments zone, which indicates that the

371   Taodonggou Group mudstone deposition was influenced by hydrothermal fluids.
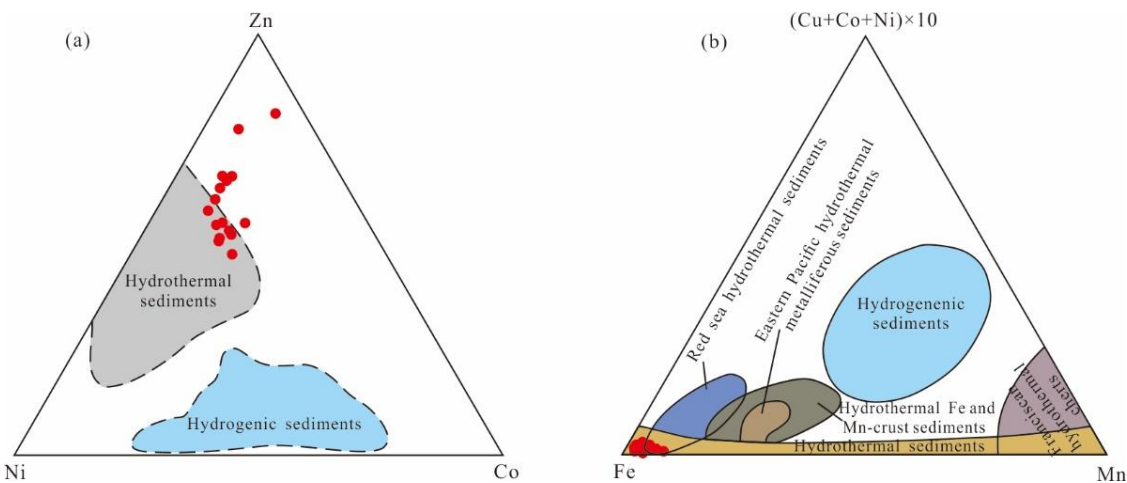
372
373   Fig.12 Zn-Ni-Co ternary diagram (a) and (Cu+Co+Ni) ×10-Fe-Mn ternary diagram (b) (modified after You et al., 2019)

374   **5.4 Tectonic setting**

375   Sedimentary rocks of different tectonic settings have prominent differences in element composition and content, so the

376   geochemical characteristics of sedimentary rocks can be used to reflect the tectonic setting of sedimentary basins

377   (Kroonenberg, 1992).

378   The elements Co, Th, Sc, Zr and La are relatively stable and less affected by geological activities such as weathering,

379   transportation and deposition. Therefore, the La-Th-Sc ternary diagram and Th-Co-Zr/10 ternary diagram can be utilized to

380   distinguish the tectonic setting during the formation of sediments (Bhatia and Crook, 1986; Cai et al., 2022). Based on the

381   La-Th-Sc ternary diagram (Fig. 13a), most of the data points fall in the continental island arc region, and on the Th-Co-Zr/10

382   ternary diagram (Fig. 13b), almost all the data points fall in the continental island arc and oceanic island arc regions. This

383   indicates that the tectonic setting of the source area of the Taodonggou Group is continental island arc and oceanic island arc.

384   Additionally, previous studies have shown that SiO_2, TiO_2, Al_2O_3/SiO_2 and Fe_2O_3+MgO are also important parameters

385   for identifying the source tectonic setting. Cross plots of Al_2O_3/SiO_2 and Fe_2O_3+MgO, TiO_2 and Fe_2O_3+MgO, and SiO_2 and

386   Al_2O_3/SiO_2 are often employed to recognize the tectonic setting (Bhatia, 1983; Li et al., 2020; Roser and Korsch, 1988). Based

387   on cross plot of Al_2O_3/SiO_2 and Fe_2O_3+MgO (Fig.13c), all data points are distributed around continental island arc and oceanic

388   island arc, which is consistent with cross plot of TiO_2 and Fe_2O_3+MgO (Fig. 13d) and cross plot of SiO_2 and Al_2O_3/SiO_2 (Fig.

389   13e). Therefore, the tectonic setting of Taodonggou Group mudstone source area is continental island arc and oceanic island

390   arc.
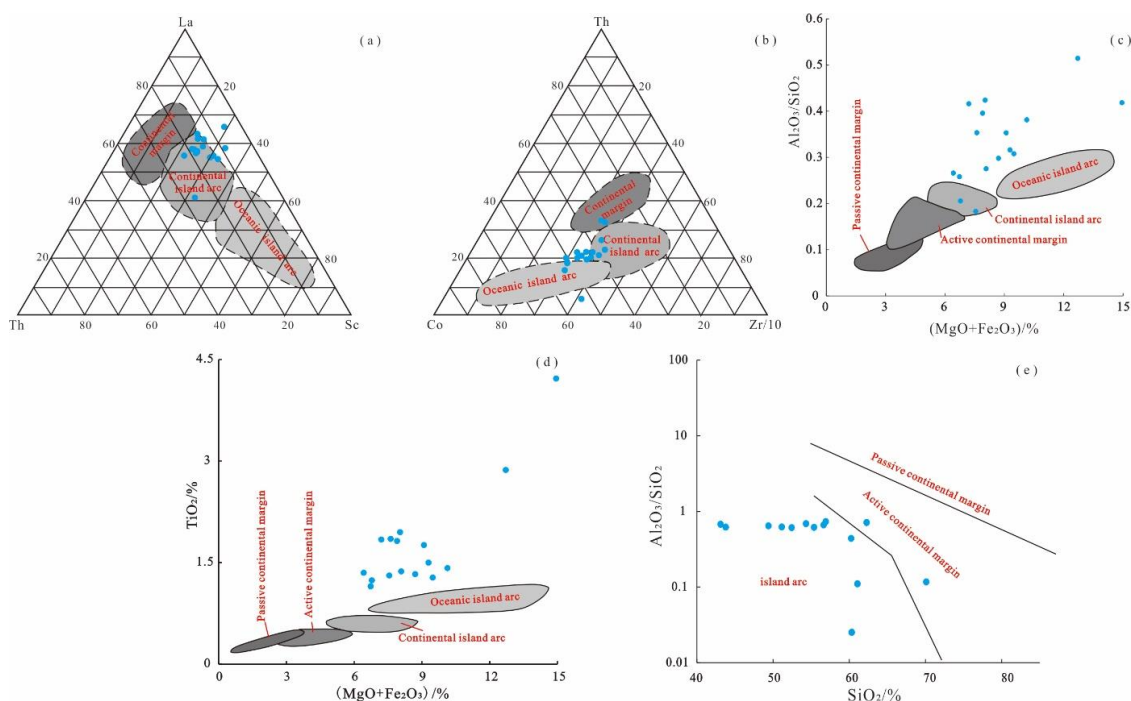
391   Fig.13 Tectonic setting of source area in Taodonggou Group mudstone: (a) La-Th-Sc ternary diagram (modified after Zhu et al., 2021); (b) Th-

392   Co-Zr/10 ternary diagram (modified after Zhu et al., 2021); (c) cross plot of Al_2O_3/SiO_2 and Fe_2O_3+MgO (modified after Bhatia, 1983); (d) cross

393   plot of TiO_2 and Fe_2O_3+MgO (modified after Bhatia, 1983); (e) cross plot of SiO_2 and Al_2O_3/SiO_2 (modified after Roser and Korsch, 1988)

5.5 Source sink system and evolution history of lake basin

396   Based on the above analysis of the source and sedimentary environment of Taodonggou Group mudstone, the

397   geochemical profile of Taodonggou Group in Well YT1 is drawn in this study (Fig. 14). According to Fig. 14 and previous

398   studies on organic matter input of Taodonggou Group mudstone (Miao et al., 2021), the lake basin evolution of Taodonggou

399   Group mudstone can be classified into three stages.

400   In the early of Taodonggou Group, Bogda Mountain began to rise but did not emerge from the water surface. The

401   sediment source is mainly from North Tianshan and Kelameili Mountain, and the secondary source area is the Jueluotage

402   Mountain in the south of the Turpan-Hami basin. The stratum of Taodonggou Group was deposited in a warm and humid

403   paleoclimate with high weathering intensity and stable input of terrigenous detritus. In addition, the sedimentary water body

404   is deep at this time, which is a deep lake environment of brackish water and dyoxic. Furthermore, the content of low aquatic

405   organisms in the lake basin at this stage is low, and the input of organic matter is mainly from terrestrial higher plants (Miao

406   et al., 2021). For this reason, a set of high-quality hydrocarbon source rocks with organic matter type III have been deposited

407   (Fig.15a).

408   In the middle of Taodonggou Group, with the continuous uplift of Bogda Mountain and hydrothermal activity, the climate

409   changed into a hot and humid paleoclimate, the weathering degree further increased, and the input of terrigenous detritus

410   increased. The provenance area is Bogda Mountain and Jueluotage Mountain. In addition, during this period, the sedimentary

411   center gradually transferred to the Taibei sag, and the sedimentary water body became shallow, which was a dyoxic

412   intermediate depth lake environment. Due to the nutrients brought by hydrothermal activities, the lower algae multiplied

413   during this period, and the salinity of the sedimentary water body became lower, becoming a freshwater environment, and

414   thus, depositing a set of high-quality II_2 organic source rocks.

415

416   Figure. 14 The geochemical profile of the Taodonggou Group in YT1 well

417

418   Figure 15 Middle Permian source sink system and lake basin evolution history of Turpan-Hami basin: (a) Early Taodonggou Group; (b) Middle

419   Taodonggou Group; (c) Late Taodonggou Group

420   In the late of Taodonggou Group, the uplift of Bogda Mountain basically stopped, and the climate changed to a warm

421   and humid paleoclimate again. The weathering degree was high, and the input of terrigenous debris was reduced. The

422   provenance areas were still Bogda Mountain and Jueluotage Mountain. At this time, the sedimentary center was basically

423   transferred to the Taibei Sag. During this period, the salinity of the sedimentary water body was high, and the sedimentary

424   water body became deeper. It was a deep lake environment with dyoxic and brackish water. A set of high-quality source rocks

425   of type III organic matter was deposited in this stage.

426   **6 Conclusion**

427   Through the mineral composition and element geochemical analysis of the Taodonggou Group mudstone, the following

428   understandings have been obtained:

429   (1) The Taodonggou Group mudstone minerals are mainly clay and quartz, and can be classified into 4 petrographic

430   types according to their mineral fractions.

431   (2) The Taodonggou Group mudstone was deposited in a warm, humid and hot paleoclimate, with strong weathering, the

parent rocks of the Taodonggou Group mudstone are two types of felsic volcanic rocks and andesites, with weak sedimentary sorting and recycling, and better-preserved source information.

(3) The Taodonggou Group mudstone were deposited in dyoxic freshwater-brackish water bodies, semi-deep lakes and deep lakes, with stable input of terrigenous debris and slower deposition rates. And in middle of the Taodonggou Group deposition influenced by hydrothermal activity, the tectonic setting of the Taodonggou Group source area is continental island arc and oceanic island arc.

(4) The evolution of the Middle Permian lake basin in the Turpan-Hami Basin can be divided into three stages: In the early part of the deposition of Taodonggou Group the depocenter was in the Bogda area. At this time the area that became Mt Bogda was not exposed and a succession of high-quality type-III source rocks was widely deposited in the basin. In the middle of the deposition of the Taodonggou Group the depocenter gradually migrated to the Taibei Sag. At this time the Mt Bogda area underwent uplift, and, together with hydrothermal activity, a succession of type-II source rocks was widely deposited in the basin. In the late part of the Taodonggou Group, uplift of the Mt Bogda area ceased and the depocenter transferred entirely to the Taibei Sag.

Data availability

Data will be made available on request.

Acknowledgement

This study was supported by National Major Science and Technology Project of China (grant nos. 2016ZX05066001-002; 2017ZX05064-003-001; 2017ZX05035-02 and 2016ZX05034-001-05), Innovative Research Group Project of the National Natural Science Foundation of China (grant nos. 41872135 and 42072151), PetroChina Science and Technology Project (grant nos. 2021DJ0602). We thank Hangzhou Yanqu Information Co., Ltd, Key Laboratory of natural gas accumulation, China National Petroleum Corporation and development and Beijing Orient Smart for providing testing samples and test equipments, as well as our colleagues' useful suggestions.

Author contribution

Miao H. and Guo J.Y. designed experiments, Wang Y.B. and Jiang Z.X. revised the first draft of the manuscript, Guo J. Y., Wang Y.B. and Jiang Z.X. provided financial support, Miao H. and Zhang C.J. provided language services and figure production, Li C.M. investigated and revised the ideas of the article, and Miao H. prepared the manuscript with your contributions. All authors contributed to the review of the manuscript.

Competing interests

The contact author has declared that none of the authors has any competing interests.

References

Algeo, T.J.; Ingall, E., 2007. Sedimentary Corg:P ratios, paleocean ventilation, and Phanerozoic atmospheric pO2.

463   Palaeogeogr. Palaeoclimatol. Palaeoecol. 256 (3–4), 130–155.

464   Algeo, T. J.; Maynard, J. B., 2004. Trace-element behavior and redox facies in core shales of Upper Pennsylvanian Kansas-

465   type cyclothems. Chem. Geol. 206(3-4), 289-318.

466   Allègre, C. J.; Minster, J. F., 1978. Quantitative models of trace element behavior in magmatic processes. Earth Planet. Sci.

467   Lett. 38, 1–25,

468   Basu, A.; Bickford, M. E.; Deasy, R., 2016. Inferring tectonic provenance of siliciclastic rocks from their chemical

469   compositions: A dissent. Sediment. Geol. 336, 26−35.

470   Bhatia, M. R., 1983. Plate tectonics and geochemical composition of sandstones. J. Geol. 91, 611– 627.

471   Bhatia, M. R.; Crook, K. A. W., 1986. Trace element characteristics of graywackes and tectonic setting discrimination of

472   sedimentary basin. Contrib. Mineral. Petrol. 92, 181–193.

473   Cai, Y. L. ; Ouyang, F.; Luo, X. R.; Zhang, Z. L.; Wen, M. L.; Luo, X. N.; Tang, R., 2022. Geochemical Characteristics and

474   Constraints on Provenance, Tectonic Setting, and Paleoweathering of Middle Jurassic Zhiluo Formation Sandstones in the

475   Northwest Ordos Basin, North-Central China. Minerals 12(5), 603.

476   Cao, L.; Zhang, Z. H.; Zhao, J. Z.; Jin, X.; Li, H.; Li, J. Y.; Wei, X. D., 2021. Discussion on the applicability of Th/U ratio for

477   evaluating the paleoredox conditions of lacustrine basins. International Journal of Coal geology. 248, 103868.

478   Cao, J.; Yang, R. F.; Yin, W.; Hu, G.; Bian, L. Z.; Fu, X. G., 2018. Mechanism of Organic Matter Accumulation in Residual

479   Bay Environments: The Early Cretaceous Qiangtang Basin, Tibet. Energy & Fuels 32(2), 1024-1037.

480   Carroll, A.; Graham, S.; Hendrix, M.; Ying, D.; Zhou; D..1995. Late Paleozoic tectonic amalgamation of northwestern China:

481   sedimentary record of the northern Tarim, northwestern Turpan, and southern Junggar basins.Geol. Soc. Am. Bull. 107, 5,

482   571-594.

483   Carroll, A.; Liang, Y. H.; Graham, S.; Xiao, X. H.; Hendrix, S.; Chu, J. C.; McKnight, L., 1990. Junggar basin, northwest

484   China: trapped Late Paleozoic Ocean. Tectonophysics 181, 1–14.

485   Deditius, A., 2015. Arsenic Environmental Geochemistry, Mineralogy, and Microbiology. Reviews in Mineralogy and

486   Geochemistry, vol 79. Economic Geology, 110, 7, 1905-1907.

487   Essefi, E., 2021. Geochemistry and mineralogy of the sebkha Oum El Khialate evaporites mixtures, southeastern Tunisia.

488   Resource Geology, 71, 3, 242-249.

489   Floyd, P. A.; Leveridge, B. E., 1987. Tectonic environment of the Devonian Gramscatho Basin, South cornwall: framework

490   mode and geochemical evidence from turibiditic sandstones. Journal of the Geological Society, 144, 4, 531-542.

491   Gehrels, G. E.; Valencia, V. A.; Ruiz, J., 2008. Enhanced precision, accuracy,efficiency, and spatial resolution of U-Pb ages

492   by laser ablation-multicollector-inductively coupled plasma-massspectrometry. Geochem., Geophys., Geosyst. 9, 3, 1– 13.

493   Glaser, K. S.; Miller, C. K.; Johnson, G. M.; Kleinberg, R. L.; Pennington, W. D., 2014. Seeking the sweet spot: Reservoir

494   and completion quality in organic shales. Oilfield Review 25, 16–29.

495   Greene, T. J.; Carroll, A. R.; Wartes, M.; Graham, S. A .; Wooden, J. L., 2005. Integrated provenance analysis of a complex

496   orogenic terrane: Mesozoic uplift of the Bogda Shan and inception of the Turpan-Hami Basin, NW China. Journal of

497   Sedimentary Research 75, 20, 251-267.

498   Guo, Z.; Zhang, Z.; Wu, C.; Fang, S.; Zhang, R., 2006. The Mesozoic and Cenozoic exhumation history of Tianshan and

499   comparative studies to the junggar and Altai mountains Acta Geol. Sin. 80, 1, 1-15

500   Hatch, J.R.; Leventhal, J.S., 1992. Relationship between inferred redox potential of the depositional environment and

501   geochemistry of the Upper Pennsylvanian (Missourian) Stark shale member of the Dennis Limestone, Wabaunsee County,

502   Kansas, USA. Chem. Geol. 99, 65–82.

503   Herkat, M.; Ladjal, A., 2013. Paleobathymetry of foraminiferal assemblages from the Pliocene of the Western Sahel (North-

504   Algeria). Palaeogeography Palaeoclimatology 374, 144-163.

505   Hu, F.; Meng, Q.; Liu, Z., 2021. Mineralogy and element geochemistry of oil shales in the Lower Cretaceous Qingshankou

506   Formation of the southern Songliao Basin, northeast China: implications of provenance, tectonic setting, and

507   paleoenvironment. ACS Earth Space Chem. 5, 365−380.

508   Ji, H.; Tao, H.; Wang, Q.; Qiu, Z.; Ma, D.; Qiu, J.; Liao P., 2018. Early to middle Jurassic tectonic evolution of the Bogda

509   mountains, northwest China: evidence from sedimentology and detrital zircon geochronology. J. Asian Earth Sci., 153, 57-74.

510   Jiang, S. H.; Li, S. Z.; Somerville, I. D.; Lei, J. P; Yang, H. Y., Carboniferous-Permian tectonic evolution and sedimentation

511   of the Turpan-Hami Basin, NW China: Implications for the closure of the Paleo-Asian Ocean. J. Asian Earth Sci., 113, 644-

512   655.

513   Kidder, D. L.; Erwin, D. H., 2001. Secular distribution of biogenic silica through the phanerozoic: Comparison of silica-

514   replaced fossils and bedded cherts at the series level. J. GEOL. 109, 4, 509-522.

515   Korobkin, V. V.; Buslov, M. M., 2011. Tectonics and geodynamics of the western Central Asian Fold Belt (Kazakhstan

516   Paleozoides). Russian Geology and Geophysics, 52, 12, 1600-1618.

517   Kröner, S. R.; McLennan, S. M., 1985. The Continental Crust: Its Composition and Evolution; Blackwell: Oxford, 312.

518   Kroonenberg, S.B., 1992. Effect of provenance, sorting and weathering on the geochemistry of fluvial sands from different

519   tectonic and climatic environments. In Proceedings of the 29th International Geological Congress, Part A, Kyoto, Japan, 24

520   August–3 September, 69, 81.

521   Lerman, A.; Baccini, P., 1978. Lakes: Chemisty, Geology, Physics. Springer-Verlag, New York.

522   Li, C. M.; Liu, J. T.; Ni, L. B.; Fan, S. W., 2021. Characteristics of deep geological structure and petroleum exploration

523   prospect in Turpan-Hami Basin. China Petroleum Exploration, 26, 4, 44-57(In Chinese with English abstract).

524   Li, Y. J. ; Sun, P. C.; Liu, Z. J.; Yao, S. Q.; Xu, Y. B.; Liu, R., 2020. Geochemistry of the Permian Oil Shale in the Northern

525   Bogda Mountain, Junggar Basin, Northwest China: Implications for Weathering, Provenance, and Tectonic Setting. ACS Earth

526   and Space Chemistry4, 8, 1332-1348.

527   Li, Y. L.; Shan, X.; Gelwick, K. D.; Yu, X. H.; Jin, L. N.; Yao, Z. Q.; Li, S. L.; Yang, S. Y., 2022. Permian mountain building

528   in the bogda mountains of NW China. International Geology Review, 2048270.

529   Li, W.; Hu, J.; Li, D.; Liu, J.; Sun, Y.; Liang, J., 2007. Analysis of the late Paleozoic and Mesozoic paleocurrents and It's

530   constructional significance of the northern Bogdashan, Xinjiang. Acta Sedimentol. Sin., 25,2, 283-292.

531   Liu, D.; Zhang, C.; Yao, E.; Song, Y.; Jiang, Z.; Luo, Q., 2017. What generated the Late Permian to Triassic unconformities

532   in the southern Junggar Basin and western Turpan Basin; tectonic uplift, or increasing aridity? Palaeogeogr. Palaeoclimatol.

533   Palaeoecol., 468, 1-17.

534   Liu, D.; Kong, X.; Zhang, C.; Wang, J.; Yang, D.; Liu, X.; Wang, X.; Song, Y., 2018. Provenance and geochemistry of Lower

535   to Middle Permian strata in the southern Junggar and Turpan basins: a terrestrial record from mid-latitude NE Pangea.

536   Palaeogeogr. Palaeoclimatol. Palaeoecol., 495, 259-277.

537   Liu, G.; Zhou, D. Application of microelements analysis in identifying sedimentary environment-taking Qianjiang Formation

538   in the Jiang Han Basin as a example. Pet. Geo. Exp. 2007, 29(3), 307-311. (In Chinese with English abstract)

539   Maravelis, A. G.; Offler, R.; Pantopoulos, G.; Collins, W. J., 2021. Provenance and tectonic setting of the Early Permian

540   sedimentary succession in the southern edge of the Sydney Basin, eastern Australia. Geological J. 56, 4, 2258-2276.

541   McLennan, S. M.; Hemming, S.; McDaniel, D. K.; Hanson, G.N., 1993. Geochemical approaches to sedimentation,

542   provenance, and tectonics. Spec. Pap. Geol. Soc. Am. 284, 21−40.

543   McLennan, S. M.; Taylor, S. R.; Kröner, A., 1983. Geochemical evolution of Archean shales from South Africa I: The

544   Swaziland and Ponggola Supergroups. Precambrian Res. 22, 93– 124.

545   Miao, H.; Wang, Y. B.; Guo, J. Y.; Fu, Y.; Li, J. H., 2022. Weathering correction and hydrocarbon generation and expulsion

546   potential of Taodonggou Group source rocks in Taibei Sag in Turpan-Hami Basin. Petroleum Geology & Oilfield

547   Development in Daqing 1-11. doi:10.19597/J.ISSN.1000-3754.202204016. (In Chinese with English abstract)

548   Miao, H.; Wang, Y. B.; Guo, J. Y.; Han, W. L.; Gong, X., 2022. Evaluation of Middle Permian source rocks of the Taodonggou

549   Group in the Turpan Hami Basin. Geophysical Prospecting for Petroleum, 61, 4, 733-742. (In Chinese with English abstract)

550   Miao, H.; Wang, Y. B.; He, C.; Li, J. H.; Zhang, W.; Zhang, Y. J.; Gong, X., 2022. Fault development characteristics and

551   reservoir control in Chengbei fault step zone,Bohai Bay Basin. Lithologic Reservoirs 34, 2, 105-115(In Chinese with an

552   English abstract).

553   Miao, H.; Wang, Y. B., Ma, Z. T.; Guo, J. Y.; Zhang, Y. J., 2022. Generalized Deltalog R model with spontaneous potential

554   and its application in predicting total organ carbon content. Journal of Mining Science and Technology, 7, 4, 417-426. (In

555   Chinese with English abstract)

556   Miao, H.; Wang, Y. B.; Zhao, S. H.; Guo, J. Y.; Ni, X. M.; Gong, X; Zhang, Y. J.; Li, J. H., 2021. Geochemistry and Organic

557   Petrology of Middle Per-mian Source Rocks in Taibei Sag, Turpan-Hami Basin, China: Implication for Organic Matter

558   Enrichment. ACS Omega. 6,47, 31578-31594.

559   Miao, J. Y.; Zhou, L. F.; Deng, K.; Li, J. F.; Han, Z. Y.; Bu, Z. Q., 2004. Organic Matters from Middle Permain Source rocks

560   of Northern Xinjiang and Their Relationships with Sedimentary environments. Geochemica. 6,551-560. (In Chinese with

561   English abstract)

562   Nesbitt, H. W.; Nesbitt, G. M. Prediction of some weathering trends of plutonic and volcanic rocks based on thermodynamic

563   and kinetic considerations. Geochim. Cosmochim. Acta. 1984, 48(7), 1523-1534.

564   Nesbitt, H. W., Young, G. M., 1984. Prediction of some weathering trends of plutonic and volcanic rocks based on

565   thermodynamic and kinetic considerations. Geochim. Cosmochim. Acta. 48, 7, 1523-1534.

566   Novikov, I. S., 2013. Reconstructing the stages of orogeny around the Junggar basin from the lithostratigraphy of Late

567   Paleozoic, Mesozoic, and Cenozoic sediments. Russian Geology and Geophysics. 54, 2, 138-152.

568   Obrist-Farner, J.; Yang, W.; Hu, X. F., 2015. Nonmarine time-stratigraphy in a rift setting: an example from the Mid-Permian

569   lower Quanzijie low-order cycle Bogda Mountains, NW China. J. Palaeogeogr., 4, 1, 27-51.

570   Pinto, L.; Munoz, C.; Nalpas, T.; Charrier, R, 2010. Role of sedimentation during basin inversion in analogue modelling.

571   Journal of Structural Geology, 32, 4, 554-565.

572   Rollinson, H. R., 1993. Using Geochemical Data: Evaluation, Presentation, Interpretation; Longman Scientific Technical:

573   New York.

574   Rosenthal, Y.; Lam, P.; Boyle, E. A.; Thomson, J., 1995. Authigenic cadmium enrichments in suboxic sediments: precipitation

575   and postdepositional mobility - sciencedirect. Earth & Planetary Science Letters 132, 1-4, 99-111.

576   Roser, B. P.; Korsch, R. J., 1988. Provenance Signatures of Sandstone-mudstone suites determined using discriminant

577   functiom analysis of major-element data. Chem. Geol. 67, 119– 139.

578   Ross, Daniel J.K., Bustin, R. M., 2009. Investigating the use of sedimentary geochemical proxies for paleoenvironment

579   interpretation of thermally mature organic-rich strata: Examples from the Devonian–Mississippian shales, Western Canadian

580   Sedimentary Basin. Chem. Geol. 260, 1–19.

581   Schoepfer, S. D.; Shen, J.; Wei, H. Y.; Tyson, Richard V.; Ingall, E.; Algeo, T. J., 2015. Total organic carbon, organic

582   phosphorus, and biogenic barium fluxes as proxies for paleomarine productivity. Earth Sci. Rev. 149, 23–52.

583   Shao L, Li WH, Yuan MS (1999) Characteristic of sandstone and its tectonic implications of the Turpan Basin. Acta

584   Sedimentologica Sinica 17(3): 435–441.

585   Shao L, Stattegger K, Garbe-Schoenberg C (2001) Sandstone petrology and geochemistry of the Turpan Basin (NW China):

586   implications for the tectonic evolution of a Continental Basin. Journal of Sedimentary Research 71(1): 37–49. (In Chinese

587   with English abstract)

588   Shi, J.; Zou, Y. R.; Cai, Y. L.; Zhan, Z. W.; Sun, J. N.; Liang, T.; Peng, P. A., 2021. Organic matter enrichment of the Chang 7

589   member in the Ordos Basin: Insights from chemometrics and element geochemistry. Marine Petroleum Geology, 134, 105306.

590   Shi, Y. Q; Ji, H. C.; Yu, J. W; Xiang, P. F.; Yang, Z. B; Liu, D. D., 2020. Provenance and sedimentary evolution from the

591   Middle Permian to Early Triassic around the Bogda Mountain, NW China: A tectonic inversion responding to the

592   consolidation of Pangea. Mar. Pet. Geol. 114, 104169.

593   Shu, L.; Wang, B.; Zhu, W.; Guo, Z.; Charvet, J.; Zhang, Y., 2011. Timing of initiation of extension in the Tianshan, based on

594   structural, geochemical and geochronological analyses of bimodal volcanism and olistostrome in the Bogda Shan (NW China).

595   Int. J. Earth Sci., 100 ,7 , 1647-1663.

596   Song, J.; Bao, Z.; Zhao, X. M.; Gao, Y. S.; Song, X. M.; Zhu, Y. Z.; Deng, J.; Liu, W.; Wang, Z. C.; Ming, C. D.; Meng, Q.

597   K.; Zhang, L.; Mao, S. W.; Zhang, Y. L.; Yu, X.; Wei, M. Y., 2018. Sedimentology and geochemistry of Middle–Upper Permian

598   in northwestern Turpan–Hami Basin, China: Implication for depositional environments and petroleum geology. Energy

599   Exploration & Exploitation 36,4 , 910-941.

600   Sun, G. ; Liu, Y., 2009. The preliminary analysis of the uplift time of Bogda Mountain, Xinjiang, Northwest China. Acta

601   Sedimentol. Sin., 27, 3, 487-491.

602   Tang, W.; Zhang, Z.; Li, J.; Li, K.; Chen, Y.; Guo Z. 2014. Late Paleozoic to Jurassic tectonic evolution of the Bogda area

603   (northwest China): evidence from detrital zircon U–Pb geochronology. Tectonophysics, 626, 144-156.

604   Taylor, S. R.; Mclennan, S. M., 1985. The continental crust: Its composition and evolution. Blackwell Science Publications,

605   Oxford.

606   Thorpe, C. L.; Law, G. T. W.; Boothman, C.; Lloyd, J. R.; Burke, I. T.; Morris, K.; 2012. The Synergistic Effects of High

607   Nitrate Concentrations on Sediment Bioreduction. Geomicrobiol. J. 29, 5, 484-493.

608   Tribovillard, N., Algeo, T. J., Baudin, F., Riboulleau, A., 2012. Analysis of marine environmental conditions based on

609   molybdenum–uranium covariation—applications to Mesozoic paleoceanography. Chem. Geol. 324,46–58.

610   Tribovillard, N.; Algeo, T. J.; Lyons, T.; Riboulleau, A., 2006. Trace metals as paleoredox and paleoproductivity proxies: an

611   update. Chemical Geology 232, 1–2, 12–32.

612   Trbovillard, N. P.; Desprairies, A; Lallier-verges, E.; Bertrand, P.; Moureau, N.; Ramdani, A.; Ramanampiso, L., 1994.

613   Geochemical study of organic-matter rich cycles from the Kimmeridge Clay Formation of Yorkshire (UK): productivity versus

614   anoxia. Palaeogeography, Palaeoclimatology, Palaeoecology, 108,1-2,165-181.

615   Wartes, M. A.; Carroll, A. R.; Greene, T. J., 2002. Permian sedimentary record of the Turpan-Hami basin and adjacent regions,

616   northwest China: Constraints on postamalgamation tectonic evolution. Geological Society of America Bulletin, 114,2, 131-

617   152.

618   Wang, A., Wang, Z., Liu, J., Xu, N., Li, H., 2021. The Sr/Ba ratio response to salinity in clastic sediments of the Yangtze River

619   Delta. Chem. Geol. 559, 119923.

620   Wang, L., 1996. Sediment flux and mechanism for the uplifting of the mountain system around the Junggar inland basin

621   Sediment. Geol. Tethyan Geol., 16, 3, 39-46.

622   Wang, J.; Cao, Y. C.; Wang, X. T.; Liu, K. Y.; Wang, Z. K.; Xu, Q. S.,2018. Sedimentological constraints on the initial uplift

623   of the West Bogda Mountains in Mid-Permian. Sci. Rep. 8, 1453.

624   Wang, J.; Wu, C.; Li, Z.; Zhu, W.; Zhou, T.; Wu, J.; Wang, J., 2018. The tectonic evolution of the Bogda region from Late

625   Carboniferous to Triassic time: evidence from detrital zircon U–Pb geochronology and sandstone petrography. Geol. Mag.

626   155, 5, 1063-1088.

627   Wang, J.; Wu, C.; Zhou, T.; Zhu, W.; Zhou, Y.; Jiang, X.; Yang, D., 2019. Source-to-Sink analysis of a transtensional rift Basin

628   from syn-rift to uplift stages. J. Sediment. Res. 89, 4, 335-352.

629   Wang, J. L.; Wu, C. D.; Zhou, T. Q.; Zhu, W.; Li, X. Y.; Zhang, T., 2019. Source and sink evolution of a Permian–Triassic

630   rift–drift basin in the southern Central Asian Orogenic Belt: Perspectives on sedimentary geochemistry and heavy mineral

631   analysis. Journal of Asian Earth Sciences 181, 103905.

632   Wang, Z. W. ; Yu, F .; Wang, J . ; Fu, X. G .; Chen, W. B. ; Zeng, S. Q.; Song, C. Y., 2021. Palaeoenvironment evolution and

633   organic matter accumulation of the Upper Triassic mudstone from the eastern Qiangtang Basin (Tibet), eastern Tethys. Marine

634   and Petroleum Geology 130, 105113.

635   Wronkiewicz, D. J.; Condie, K. C., 1987. Geochemistry of archean shales from the witwatersrand supergroup, south Africa:

636   Source-area weathering and provenance. Geochimica Cosmochimica Acta 51, 9, 2401-2416.

637   Wei, H.; Chen, D. Z.; Wang, J. G.; Yu, H.; Tucker, M. E., 2012. Organic accumulation in the lower Chihsia Formation (Middle

638   Permian) of South China: Constraints from pyrite morphology and multiple geochemical proxies. Palaeogeogr. Palaeoclimatol.

639   Palaeoecol. 353, 73-86.

640   Wu, C.; Li, H. W.; Sheng, S. Z.; Chen, T.; Shi, X. F.; Jiang, M. L., 2021. Characteristics and main controlling factors of

641   hydrocarbon accumulation of Permian-Triassic in Lukeqin structural zone, Tuha Basin. China Petroleum Exploration 26, 4,

642   137-148. (In Chinese with English abstract)

643   Xiong, X. H.; Xiao, J. F., 2011. Geochemical Indicators of Sedimentary Environments—A Summary. Earth and Environment

644   39, 3, 405-414. (In Chinese with English abstract)

645   Xu, C. ; Shan, X. L. ; Lin, H. M .; Hao, G. L.; Liu, P .; Wang, X. D.; Shen, M. R. ; Rexiti, Y. ; Li, K.; Li, Z. S.; Wang, X. M.;

646   Du, X. D.; Zhang, Z.W.; Jia, P. M.; He, W. T., 2022. The formation of early Eocene organic-rich mudstone in the western

647   Pearl River Mouth Basin, South China: Insight from paleoclimate and hydrothermal activity. International Journal of Coal

648   geology 253, 103957.

649 Yang, Y.; Song, C.; He, S., 2015. Jurassic tectonostratigraphic evolution of the Junggar basin, NW China: a record of Mesozoic

650 intraplate deformation in Central Asia. Tectonics 34, 1, 86-115.

651 You, J.; Liu, Y. ; Zhou, D .; Zheng, Q.; Vasichenko, K .; Chen, Z., 2019. Activity of hydrothermal fluid at the bottom of a lake

652 and its influence on the development of high-quality source rocks: Triassic Yanchang Formation, southern Ordos Basin, China.

653 Australian Journal of Earth Sciences 67, 1, 115-128.

654 Zhang, C.; He, D.; Wu, X.; Shi, X.; Luo, J.; Wang, B.; Yang, G; Guan, S.; Zhao, X., 2006. Formation and evolution of

655 multicycle superimposed basins in Junggar Basin. China Petrol. Explor. 11, 1, 47-58.

656 Zhang, K. ; Song, Y. ; Jiang, S. ; Jiang, Z. X. ; Jia, C. Z. ; Huang, Y. Z.; Wen, M .; Liu, W. W .; Xie, X. L.; Liu, T. L.; Wang,

657 P. F.; Shan, C. A.; Wu, Y. H., 2019. Mechanism analysis of organic matter enrichment in different sedimentary backgrounds:

658 A case study of the Lower Cambrian and the Upper Ordovician-Lower Silurian, in Yangtze region. Mar. Petrol. Geol. 99,

659 488–497.

660 Zhang, S.; Liu, C.; Bai, J.; Wang, J.; Ma, M.; Guan, Y.; Peng, H., 2019. Provenance variability of the Triassic strata in the

661 Turpan-Hami basin: detrital zircon record of Indosinian tectonic reactivation in eastern Tianshan. Acta Geol. Sin. 93, 6, 1850-

662 1868.

663 Zhang, S. C.; Zhang, B. M.; Bian, L. C.; Jing, Z. J.; Wang, D. R.; Zhang, X. Y.; Gao, Z. Y.; Chen, J. F., 2005. Development

664 constraints of marine source rocks in China. Earth Sci. Frontiers 12, 3, 39-48. (In Chinese with English abstract)

665 Zhao, R.; Zhang, J. Y.; Zhou, C. M.; Zhang, Z. J.; Chen, S.; Stockli, D.F.; Olariu, C.; Steel, R.; Wang, H., 2020. Tectonic

666 evolution of Tianshan-Bogda-Kelameili mountains, clastic wedge basin infill and chronostratigraphic divisions in the source-

667 to-sink systems of Permian-Jurassic, southern Junggar Basin. Mar. Petrol. Geol. 114, 104200.

668 Zhao, B. S.; Li, R. X.; Qin, X. L.; Wang, N.; Zhou, W. ; Khaled, A .; Zhao, D.; Zhang, Y. N.; Wu, X. L.; Liu, Q., 2021.

669 Geochemical characteristics and mechanism of organic matter accumulation of marine-continental transitional shale of the

670 lower permian Shanxi Formation, southeastern Ordos Basin, north China. Journal of Petroleum Science and Engineering, 205,

671 108815.

672 Zhu, Q. M.; Lu, L. F.; Pan A. Y.; Tao, J. Y.; Ding, J. H.; Liu, W. L.; Li, M. W., 2021. Sedimentary environment and organic

673 matter enrichment of the Lower Cambrian Niutitang Formation shale, western Hunan Province, China. Petroleum Geology

674 & Experiment 43, 5, 797-854. (In Chinese with English abstract)

675 Zhu, X.; Wang, B; Chen, Y.; Liu, H. S., 2019. Constraining the Intracontinental Tectonics of the SW Central Asian Orogenic

676 Belt by the Early Permian Paleomagnetic Pole for the Turfan-Hami Block. Journal of Geophysical Research-solid earth, 124,

677 12, 12366-12387.